Highlights

Minimizing concrete consumption in slabs by optimizing column locations

Yakov Zelickman, Oded Amir

- Efficient gradient-based optimization of column locations considering deflection, shear and moment constraints
- Concrete savings of up to 50% are achieved by optimizing the column locations
- Optimal locations of supporting columns are not trivial
- Even very minor updates of column locations may result in significant concrete savings
- The trade-off between structural efficiency and architectural freedom is demonstrated and discussed

Minimizing concrete consumption in slabs by optimizing column locations

Yakov Zelickman[a], Oded Amir[a]

[a]*Technion - Israel Institute of Technology, Haifa, 3200003, Israel*

Abstract

Reducing concrete consumption is important as part of the global effort of fighting the climate change, and specifically in concrete flat slabs as these are among the largest cement consumers. In this study we investigate the sensitivity of flat slabs' thickness to the column locations and search for optimal column layouts. We develop an efficient gradient-based optimization of column locations, that minimizes the slabs' thickness with constraints on the deflections, moments, and shear forces. The results show that the columns' optimal locations are not trivial and that the slab thickness is very sensitive to the columns' exact locations. Thus, concrete savings in slabs of up to 20% are possible with minor modification to traditional layouts of columns, and up to 50% with more pronounced updates, which emphasizes the importance of early collaboration between architects and engineers. The results expose the critical trade-off between structural efficiency and architectural freedom and demonstrate the potential of formal optimization in structural design.

Keywords: Concrete floors, Structural optimization, Columns layout, Structural Engineering

1. Introduction

Concrete is one of the most highly consumed materials in the world, being the third largest source of carbon dioxide emissions [1]. Considering structural elements in buildings, a large portion of concrete is used in slabs. In fact, several recent studies investigated the usage of cement in different structural components in buildings and infrastructure, and it was shown that slabs hold the highest share of cement [2, 3, 4]. Therefore, reducing the volume of concrete in slabs has high potential for reducing the environmental burden caused by cement production [4]. Moreover, slabs in buildings contribute significantly to the mass of the structure, and consequently to the gravitational and earthquake loads that the building must withstand. Thus, reducing the slabs' mass will lead to further concrete savings in other structural elements, such as columns and foundations.

Structural optimization is a design approach where a structural design problem is formulated as a constrained minimization problem and solved with mathematical programming tools [5]. It has been shown as an effective design tool in many branches of engineering that often leads to significant savings

in material and improvements in performance [6, 7]. Thus, structural optimization is a promising design approach to reduce the environmental impact of concrete structures [4, 8, 9].

Optimization of concrete floor systems where the column locations are fixed, is the subject of many studies, aiming to minimize objective functions such as material consumption, cost, and environmental footprint. To name a few, Varaee and Ahmadi-Nedushan [10] minimized the cost of uni-directional flat plates with a single span, whereas cost minimization of flat plates with arbitrary shapes can be found in [11]. Cost optimization of a waffle slab was presented by Olawale et al. [12], who formulated a compact geometrical parametrization and therefore used a Genetic Algorithm (GA) for solving the optimization. Richer parametrization, that allows the shape of the ribs to vary was recently presented by Ismail and Mueller [13]. Some papers proposed optimization methods that consider multiple options for the floor structural system, for example [14].

The layout of columns, and more generally the layout of supports, significantly affects the structural response of plates. Therefore, optimizing the locations of the supporting elements is an effective way of reducing the environmental footprint of concrete slabs [15, 16]. In an early paper, the authors minimize the cost of a rectangular flat plate by optimizing a comprehensive set of parameters, including the span lengths [17]. Therein, a two-step framework is presented where the floor is optimized using GA for given span lengths, which are then updated following a heuristic scheme. A more general rectilinear flat plate was considered in Nimtawat and Nanakorn [18], where the layout of orthogonal beams supporting a flat slab was optimized, for a given layout of columns and general rectilinear floor geometries. In this study, the maximal span is prescribed inherently by the design space, where the total length of the beams was minimized using GA. A rectilinear floor was also presented in Shaw et al. [19], where the authors used GA to optimize the layout of prefabricated slab elements and the supporting columns. In a more recent study, the authors use Ant Colony Optimization to optimize the layout of an orthogonal-supported rectilinear building [20]. Additionally, the floor plan is optimized with a constraint on the total floor area. The objective function includes the cost of the frames and the slabs, and the eccentricity between the mass- and the rigidity- centers. Recently, Building Information Modelling (BIM) was coupled with Finite Element (FE) analysis and GA to create a framework for preliminary design of concrete structures, including spacing between column grid-lines [15]. In another recent study, the authors use Monte Carlo method to find the optimal locations of supports of concrete plates, minimizing the strain energy, reinforcement steel and maximal deflection [21].

All studies that were mentioned so far, and most of the available literature that discusses optimization of concrete floor systems, adopts meta-heuristic and zero-order optimization algorithms, which allow to cope with the non-differentiable and discontinuous constraints, but also becomes very expensive computationally in high dimensional optimization [22]. Therefore, the design space includes a

small number of design variables, restricting the optimization to regular layouts of columns or to a limited number of columns.

Gradient-based optimization algorithms are more likely to converge to local minima than meta-heuristic algorithms, but offer superior numerical efficiency and therefore were also considered in many studies. In a straightforward approach for optimization of supports' locations, the coordinates of the supported nodes are being optimized [23, 24]. This approach requires constant remeshing and control over the FE mesh, and therefore is numerically expensive and may encounter stability issues. Another approach, that uses a SIMP-like parametrization, was proposed by Buhl [25]. Mathematical continuity is obtained by adding springs to all nodes and assigning penalized topological design variables to each one of the springs. Thus, by adding a constraint on the sum of the topological design variables, the most effective springs remain, designating the optimal locations. This approach was adopted in several studies, for example Jihong and Weihong [26], Denli and Sun [27], and recently used by Meng et al. [28] to minimize the compliance of plate roof structures. Another recent paper presents the stiffness projection method for support location optimization, which is both numerically efficient and mesh-independent, and therefore much less prone to convergence to local minima than the other gradient-based approaches [29]. Similarly to Meng et al. [28], the formulation there includes only compliance minimization and therefore does not consider the major requirements for the design of concrete slabs, e.g. bending moments, shear forces and deflections.

From the discussion above it is apparent that existing studies on column layout optimization of concrete floors were using meta-heuristic algorithms, mainly GA. As a result, the design space is limited to a small number of design variables, and therefore the existing methods focus on a regular grid of columns and simple floor plans. On the other hand, studies that used efficient gradient-based algorithms, which result in a rich design space, consider only global structural performance and lack the necessary constraints for the structural design of concrete floors.

In this study we aim to fill this gap by proposing a gradient-based optimization for the layout of the columns in floors with arbitrary shapes, considering the major design requirements of concrete plates. Thereafter, we take advantage of the proposed explicit, efficient, and geometrically free optimization method to investigate the sensitivity of the plate thickness to the locations of columns.

Specifically, we adopt the stiffness projection method, that was presented in the authors' previous work [29], and extend it significantly by adding deflection, punching shear, and bending moment constraints, as well as explicitly minimizing the concrete volume and adding the plate thickness to the design space. As a result, the columns are not restricted to any location or pattern, which gives rise to non-trivial layouts and significant reduction in concrete mass. As expected, there is a clear trade-off between concrete volume and the architectural design freedom. Less expected is how significant are

the concrete savings when only slight changes are made to the column locations, imposing only a minor compromise on the architectural freedom. Thus, this study demonstrates the importance of close collaboration between structural engineers and architects from the preliminary design stages, when the column locations are determined.

The remainder of this paper is arranged as follows. In the next section we briefly present the mathematical model, thereafter in Section 3 we discuss the optimization formulation extensively. In Section 4 we present three numerical examples that are followed by a brief discussion and some concluding remarks in Section 5. The paper has two appendices: The first presents the analytical sensitivity analysis and the second provides some details about the implementation of the optimization method.

2. Mathematical model

In structural optimization, the mathematical model is a structural model that predicts the structural response to a given set of loads for a given set of parameters, including the design parameters. In the context of the current study, the structural model is a plate model where the supports locations and the thickness may vary throughout the optimization. We note that the mathematical model that we use in the current study was already presented and discussed extensively in our previous work [29]. Herein the mathematical model is described briefly for completeness.

The slabs are modeled with plate finite elements using Mindlin plate theory [30, 31]. Following common practice in the analysis of concrete slabs, we assume small displacements and strains as well as linear elastic behavior of the concrete. Thus, the floor is modeled with 4-noded plate elements with mixed interpolation, that are known to be accurate and insensitive to shear locking [32].

Since we optimize the locations of the columns, the boundary conditions of the slab change throughout the optimization. Generally, this class of problems suffers from several difficulties: 1) Possible discontinuity of the design space; 2) High computational cost if remeshing is used; and 3) Tendency to converge to poor local optima. Therefore, in this study we use the stiffness projection method that was presented in our previous work to overcome these challenges [29].

As the name suggests, the basic idea is to project the stiffness of the columns upon the plate's FE mesh instead of modeling the columns explicitly, which results in a certain level of approximation. However, when compared to models with compatible meshes and precise column locations, the relative error in the structural response is in the order of 1×10^{-3}, which is acceptable in the context of optimization. Thus, all nodes within a circular projection area Ω_i defined by a projection radius of η_i, have added nodal stiffness. This added stiffness equals to the column's stiffness matrix multiplied by a weight factor w_{ij} that relates the i^{th} column with the j^{th} node. Thereafter, the added nodal stiffness

matrices are assembled into a global equivalent stiffness matrix of the i^{th} column

$$\mathbf{K}_{cp,i} = \sum_{\Omega_i} w_{ij} \mathbf{K}_{c,i} \quad \text{with} \quad \Omega_i = \left\{ j | r_{ij} \leq \eta \right\}. \tag{1}$$

In the above expression, $\mathbf{K}_{cp,i}$ and $\mathbf{K}_{c,i}$ are the i^{th} column equivalent and nominal stiffness matrices; r_{ij} is the distance between the i^{th} column and the j^{th} node; and the sum operator represents assembly according the degrees of freedom of the model. Because we use gradient based optimization in this study, all functions have to be differentiable and therefore we use a smooth radial super-Gaussian function for the projection weight factors

$$\tilde{w}_{ij} = \tilde{w}\left(r_{ij}\right) = \exp\left(-0.5\left(\frac{r_{ij}}{\eta}\right)^{2\beta}\right), \tag{2}$$

where β is a parameter that controls the sharpness of the transition across the boundary of the projection area. This means that mathematically the stiffness of any column is projected onto all nodes of the FE mesh, with practically zero projection weight outside the desired projection area. To ensure that no excess stiffness is generated by the projection, we normalize the projection weights

$$w_{ij} = \frac{\tilde{w}_{ij}}{\sum_k \tilde{w}_{ik}} \quad \text{with} \quad k = [1 \ldots N_n], \tag{3}$$

where N_n is the total number of nodes. After the equivalent stiffness matrices of all columns have been computed, they are added to the plate's stiffness matrix $\mathbf{K}_p$, which results in the stiffness matrix of the supported plate, $\mathbf{K}$.

3. Optimization problem formulation

In this section, we rely on the projection-based parameterization introduced in [29] and extend the formulation significantly, such that a design-oriented problem formulation is defined. Thus, we minimize the concrete volume and consider the major service and design limit state requirements. Arranging the optimization problem into standard form, we obtain

$$
\begin{aligned}
\underset{\mathbf{X}}{\text{minimize}} \quad & f_0 = V \\
\text{s.t.} \quad & f_1 = \frac{\tilde{\delta}}{\tilde{\delta}^*} - 1 \leq 0 \\
& f_2 = \frac{\tilde{\sigma}_{ts}}{\tilde{\sigma}^*_{ts}} - 1 \leq 0 \\
& f_3 = \frac{\tilde{\mu}}{\tilde{\mu}^*} - 1 \leq 0 \\
& \tilde{\mathbf{X}}_{min} \leq \tilde{\mathbf{X}} \leq \tilde{\mathbf{X}}_{max} \\
\text{with:} \quad & \mathbf{K}\mathbf{u}_\text{s} = \mathbf{f}_\text{s} \\
& \mathbf{K}\mathbf{u}_\text{d} = \mathbf{f}_\text{d}.
\end{aligned}
\tag{4}
$$

In the formulation above: f_1 is the deflection constraint; f_2 is the shear stress constraint; and f_3 is the bending moment constraint. Another set of constraints defines the physical design space, and the equilibrium equations are considered in a nested configuration. Although the formulation is general and any number of load cases can be accommodated, in this study all examples have only two different load cases with uniformly distributed loads that correspond to service and design limit states. The service limit state and the design limit state load vectors, $\mathbf{f}_s$ and $\mathbf{f}_d$, are given by

$$
\begin{cases}
\mathbf{f}_s = \mathbf{g} + \Delta\mathbf{g} + \mathbf{q} \\
\mathbf{f}_d = 1.4\,(\mathbf{g} + \Delta\mathbf{g}) + 1.6\mathbf{q}
\end{cases},
$$

where $\mathbf{g}$, $\Delta\mathbf{g}$ and $\mathbf{q}$ are the nodal self weight, dead load, and live load vectors, respectively.

We note that including pattern loading between different bays will result in a more accurate representation of the expected loads on the floor. However, applying pattern loading requires automatic pattern recognition as the columns change their location throughout the optimization. This is not a trivial task and is beyond the scope of this study. Nevertheless, the comparison between the optimized and the reference designs is fair since all cases are loaded identically. From the perspective of the optimized column locations, uniform loading and pattern loading should result in very similar column layout, since different load patterns balance each other.

The plate forces and moments are obtained in design limit state by computing

$$
\hat{\mathbf{S}} = \mathbf{D}\mathbf{B}\mathbf{u}_d, \tag{5}
$$

where $\hat{\mathbf{S}}$ is a vector with the plate forces and moments evaluated at the Gauss points, $\mathbf{D}$ is the plate's constitutive matrix, and $\mathbf{B}$ is a differentiation matrix. The nodal forces and moments are computed using the SPR technique [33]

$$
\mathbf{S} = \left\{ \mathbf{M}^T_{xx} \quad \mathbf{M}^T_{yy} \quad \mathbf{M}^T_{xy} \quad \boldsymbol{\sigma}^T_{xz} \quad \boldsymbol{\sigma}^T_{yz} \right\}^T = \mathbf{W}^T \hat{\mathbf{S}}, \tag{6}
$$

where $\mathbf{S}$ is a vector with the nodal bending moments and transverse shear forces, and $\mathbf{W}$ is a constant transformation matrix. Finally, $\mathbf{X}$ is the normalized *mathematical* design vector, whereas $\tilde{\mathbf{X}}$ is the *physical* design vector that holds the actual design parameters that we wish to optimize.

3.1. Design Space

The purpose of the optimization is to minimize the consumed concrete by optimally locating the columns and finding the corresponding minimal thickness of the slab. Thus, for N_{col} initially defined number of columns, there are $N_{dv} = 2N_{col} + 1$ design variables, which we arrange in a physical design variables vector

$$\tilde{\mathbf{X}}^T = \left[\mathbf{x}_c^T, \mathbf{y}_c^T, h\right], \tag{7}$$

where $\mathbf{x}_c$ and $\mathbf{y}_c$ are vectors with the x and y coordinates of all columns and h is the thickness of the slab. We note that a possible extension of this work could include spatial variation of h that can lead to further volume reduction, at the price of more complicated construction. The gradient-based approach then becomes mandatory, because the number of design variables increases drastically.

The final set of constraints in Eq. (4) are the limits on the physical design variables. In the case of the thickness, the limits are straightforward: $h_{min} \leq h \leq h_{max}$, where h_{min} arises from building codes and regulations, and h_{max} is an architectural constraint. However, the limits on the variables that govern column locations are design-dependent for floors with arbitrary non-convex shapes. In this study, we require that at each design iteration, the updated location of a column will remain in the circle defined by the current location of the column and the shortest distance to the boundary, which includes both the contour of the floor and the openings. Therefore, for a column with shortest distance of d_{min}, the design limits in each direction are conservatively set to $\frac{d_{min}}{2}$, which results in the following limits

$$\left[\mathbf{x}_{c,max}, \mathbf{x}_{c,min}\right] = \mathbf{x}_c \pm \frac{1}{2}\mathbf{d}_{min}\left(\mathbf{x}_c, \mathbf{y}_c\right) \tag{8}$$

$$\left[\mathbf{y}_{c,max}, \mathbf{y}_{c,min}\right] = \mathbf{y}_c \pm \frac{1}{2}\mathbf{d}_{min}\left(\mathbf{x}_c, \mathbf{y}_c\right), \tag{9}$$

where $\mathbf{d}_{min}$ is a vector with the shortest distance from all columns to the boundary of floor.

To compute d_{min} we approximate the floor boundaries with polygons, and then place sampling points (SP) along each side of the polygons with distance of roughly $0.1[m]$ between adjacent SP. As a result, each vertex of the polygons has two SP. Thereafter we compute the distance from the column to all SP and select the two closest SP to the column. If both SP have the same location, it means that the column is closest to a vertex of the polygon and d_{min} is equal to this distance. Otherwise, d_{min} is equal to the shortest distance to the line connecting both SP.

Moreover, we use the derivatives of the shortest distance with respect to the column coordinates to identify the direction to the nearest boundary. Thus, considering for example the x coordinate of a column, a positive derivative indicates that the closest SP is somewhere to the left of the column location. Therefore, the design limit to the right may be larger and is defined by the maximal move limit value, which is discussed in Appendix B.2. A similar logic applies also to a negative sign of the derivative and when considering the y coordinate.

We note that in a case of close vicinity of a column to an ear vertex of the boundary polygon, the proposed strategy may allow the column to exit the domain. However, since the columns naturally prefer to remain strictly within the floor area, setting small enough distance between the SP resolves any related issues.

As mentioned, we distinguish between the *physical design variables*, which refers to the actual parameters that we want to find, and the *mathematical design variables*, that we solve in the optimization problem

$$\mathbf{X}^T = \left[\mathbf{r}_c^T, \mathbf{s}_c^T, \omega\right]. \tag{10}$$

The mathematical design variables are normalized and therefore linearly related to the physical design variables

$$\mathbf{X} = \mathbf{N}\tilde{\mathbf{X}}, \tag{11}$$

where $\mathbf{N}$ is the diagonal normalization matrix. The entries on the diagonal of $\mathbf{N}$ are $1/B_x$, $1/B_y$, or $1/(h_{max} - h_{min})$ for the column locations in x and y directions, and the slab thickness, respectively. This normalization generally results in more stable optimization and conveniently separates the optimization procedure from the specific geometrical parameters of the problem being solved. The limits on the mathematical design variables are obtained by normalization of the physical design limits

$$0 \le \frac{\mathbf{x}_{c,min}}{B_x} \le \mathbf{r}_c \le \frac{\mathbf{x}_{c,max}}{B_x} \le 1, \quad 0 \le \frac{\mathbf{y}_{c,min}}{B_y} \le \mathbf{s}_c \le \frac{\mathbf{y}_{c,max}}{B_y} \le 1, \quad 0 \le \omega \le 1. \tag{12}$$

3.2. Volume Objective

As stated, we wish to minimize the concrete consumption, and therefore minimize the concrete volume. We measure the concrete volume explicitly by summing the volumes of the individual finite elements

$$V = \sum_{\ell=1}^{N_\ell} hA_\ell, \tag{13}$$

where A_ℓ is the area of the ℓ^{th} finite element, and N_ℓ is the total number of elements in the FE mesh.

3.3. Deflection Constraint

Many standards define the allowed deflection in concrete elements as a fraction of their span. In general, floors have multiple spans, each possibly with different length, and therefore different areas

of a floor might have different allowed deflection. To successfully impose deflection constraints we define the relative deflection at each node δ_j as the ratio between the actual elastic downward deflection in service limit state and the allowed deflection at this node

$$\delta_j = \frac{w_j}{w_{A,j}}, \tag{14}$$

where w_j and $w_{A,j}$ are the actual and allowed deflections in z direction at the j^{th} node, respectively. The constraint aggregates all nodal relative deflections by considering the maximal relative deflection, which is approximated using a p-norm function

$$\tilde{\delta} = \left(\sum_{j=1}^{N_n} \delta_j^p \right)^{\frac{1}{p}}. \tag{15}$$

In the equation above, $\tilde{\delta}$ is the approximate maximal relative deflection, N_n is total number of nodes in the FE mesh, and p is an even number allowing to account for both positive (upward) and negative (downward) deflections. Moreover, since the deflections are quite smooth, we use a fairly high power value of $p = 30$. This approximation overestimates the real maximum, $\tilde{\delta} > \max(\boldsymbol{\delta})$, which may lead to undesired conservativeness. Therefore, the threshold value of the constraint is dynamically updated as follows

$$\tilde{\delta}^* = \frac{\tilde{\delta}}{\max(\boldsymbol{\delta})} \delta^*, \tag{16}$$

every $N_{Ic} = 5$ iterations, where the nominal required relative deflection is $\delta^* = 1.0$.

The definition of the allowed deflection follows the recommendations in Eurocode 2 (EC2) [34], where the long term deflection should be less than $\frac{1}{250}$ of the span length. Thus, assuming a long term deflection coefficient of 3.0, the allowed deflection at node j is

$$w_{A,j} = \frac{L_{eq,j}}{750}, \tag{17}$$

where $L_{eq,j}$ is the equivalent span length at this node. However, since the column locations change in every optimization iteration, the equivalent spans lengths change as well. As a result, both the deflection itself and the allowed deflection at each node are design dependent, which introduces a unique challenge for optimization of irregular column layouts.

As in [35], we wish to define the equivalent span length as the diameter of the maximal inscribed circle in a polygon defined by the surrounding columns at each point. This diameter can be approximated as $d = \sqrt{2} r_{min}$, where r_{min} is the distance to the closest column. Thus, we define the equivalent span length at any node j as follows,

$$L_{eq,j} = r_0 + \sqrt{2} r_{min,j} \quad \text{with} \quad r_{min,j} = \min_i \left(r_{ij} \right), \quad i \in [1, \ldots, N_{col}], \tag{18}$$

where $r_{min,j}$ is the distance from the j^{th} node to the closest column and r_0 is a constant value that we add to allow some minimal deflection at the supports. This allowed deflection at the columns is necessary to accommodate for the inevitable deflection at the supports, as the supports have finite stiffness, as discussed in Section 2. We chose the value $r_0 = 0.7[m]$, which allows an elastic deflection at the supports of approximately $1 \times 10^{-3}[m]$. Again, we approximate the non-differentiable distance to the closest column in Eq. (18) with a p-norm function

$$r_{min,j} \approx \left(\sum_{i}^{N_{col}} r_{ij}^{-p} \right)^{-\frac{1}{p}}. \tag{19}$$

3.4. Shear Constraint

Shear in slabs, or punching shear, is a key consideration in the design of concrete slabs and hence is added to the formulation. We define a sufficient thickness of the slab such that the punching resistance at each point can be provided by steel details only, without further thickening. Thus, following the recommendations in EC2, we will require for each node j that

$$\begin{cases} \sigma_{xz,j} \leq \nu_{Rd,max} \\ \sigma_{yz,j} \leq \nu_{Rd,max} \end{cases} \quad \text{with} \quad \nu_{Rd,max} = 0.4 \cdot 0.6 \left[1 - \frac{f_{ck}}{250} \right] f_{cd} \approx 0.2 f_{cd}. \tag{20}$$

In the expression above, $\sigma_{xz,j}$ and $\sigma_{yz,j}$ are the plate transverse shear stresses acting at node j in design limit state, $\nu_{Rd,max}$ is the maximal allowed shear stress, f_{ck} is the characteristic concrete strength (in $[Mpa]$) and f_{cd} is the compression design strength of the concrete. We note that we omit the eccentricity parameter β suggested by EC2, because the shear stresses are computed directly and thus the actual structural response is already taken into account. Similarly to the deflection constraint, we constrain the maximal shear stress rather than having separate nodal constraints. Thus, the approximate maximal shear stress is

$$\tilde{\sigma}_{ts} = \left(\sum_{j=1}^{2N_n} \sigma_{ts,j}^{p} \right)^{\frac{1}{p}} \quad \text{with} \quad \boldsymbol{\sigma}_{ts} = \begin{bmatrix} \boldsymbol{\sigma}_{xz} \\ \boldsymbol{\sigma}_{yz} \end{bmatrix}. \tag{21}$$

We note that the shear may be both positive and negative and therefore the value of the power p should be even. The threshold is updated in the same way as in the deflection constraint,

$$\tilde{\sigma}_{ts}^{*} = \frac{\tilde{\sigma}_{ts}}{\max(\boldsymbol{\sigma}_{ts})} \nu_{Rd,max}. \tag{22}$$

For convenient presentation of the results, we define the relative shear stress as the ratio between the nodal shear stress and the maximal allowed shear stress

$$\boldsymbol{\tau}_{xz} = \frac{\boldsymbol{\sigma}_{xz}}{\nu_{Rd,max}}, \quad \boldsymbol{\tau}_{yz} = \frac{\boldsymbol{\sigma}_{yz}}{\nu_{Rd,max}}. \tag{23}$$

3.5. Bending Moment Constraint

Another important design consideration in concrete elements is the bending moment capacity. In slabs, it is common that no compressive steel is needed. Thus, in this study we aim for structural depth that will subsequently allow a design with tensile steel only. Following recommendations in many design codes, such as EC2, we assume a simplified rectangular stress block with maximal height of $0.4d$, where $d = h - d_s$ is the effective structural depth and d_s is the concrete cover over the reinforcement bars. Thus, the maximal bending capacity per unit width without compressive reinforcement is given by

$$M_c = 0.32\,(h - d_s)^2\, f_{cd}. \tag{24}$$

We note that this approximation provides good agreement for $f_{cd} \leq 28[Mpa]$, especially as the moments approach M_c.

Following common practice, we take into account the torsion moments in the slab by considering the Wood and Armer (W&A) moments [36]. Thus, we combine the pure bending moments with the torsional moments to create the design moments

$$\begin{aligned} M_{rx,max} &= M_{xx} + \left|M_{xy}\right| \\ M_{rx,min} &= M_{xx} - \left|M_{xy}\right| \\ M_{ry,max} &= M_{yy} + \left|M_{xy}\right| \\ M_{ry,min} &= M_{yy} - \left|M_{xy}\right|, \end{aligned}$$

where M_{xx}, M_{yy}, M_{xy} are the plate moments in design limit state. For convenient presentation of the bending of the plate, we define the relative moment as the ratio between the nodal moments and the moments capacities. Thus, the relative $M_{rx,max}$ moment at any node j is

$$\mu_{rx,max,j} = \frac{M_{rx,max,j}}{M_c}, \tag{25}$$

and similarly for the other moments. In order to constrain all moments at all nodes, we constrain the approximate maximum relative moment

$$\tilde{\mu} = \left(\sum_{j=1}^{4N_n} \mu_j^p\right)^{\frac{1}{p}} \quad \text{with} \quad \boldsymbol{\mu} = \begin{bmatrix} \boldsymbol{\mu}_{rx,max} \\ \boldsymbol{\mu}_{rx,min} \\ \boldsymbol{\mu}_{ry,max} \\ \boldsymbol{\mu}_{ry,min} \end{bmatrix}. \tag{26}$$

Finally, the threshold value of the moment constraint is updated similarly to the shear and deflection constraints, with normalized desired threshold value $\mu^* = 1$

$$\tilde{\mu}^* = \frac{\tilde{\mu}}{\max(\boldsymbol{\mu})}. \tag{27}$$

3.6. Optimization Sequence

It was observed during our numerical experiments that often only the displacement constraint is active. Thus, in many cases the bending moment constraint and the shear constraint may be omitted. This results in much faster optimization because it spares computing $\mathbf{u}_d$ as well as the corresponding adjoint vectors, each requires solving a set of equilibrium equations which is the most expensive computational task. Obviously, one cannot know in advance whether the design limit state constraints will be active. Therefore, in this study we implemented a hierarchical optimization sequence. Initially, we optimize with the displacement constraint only and check upon convergence the resultant moment and shear distribution. In a case that both the moment and shear values are within the desired limits, the optimized design is considered as the solution of the optimization problem. Otherwise, we update the optimized design by another optimization. This time, all constraints are included and the initial design is the optimized design from the previous optimization.

3.7. Sensitivity analysis

In this study we use gradient-based optimization that allows to effectively cope with multidimensional optimization, and specifically we adopt the MMA algorithm [37]. Therefore, the derivatives of all functionals in Eq. (4) with respect to all design variables should be derived, a process that is often referred to as Sensitivity Analysis (SA). The SA of a functional f_i with respect to the *mathematical* design variables is given by

$$\frac{\partial f_i}{\partial \mathbf{X}} = \frac{\partial f_i}{\partial \tilde{\mathbf{X}}} \mathbf{N}^{-1} \tag{28}$$

where $\mathbf{N}$ is the normalization matrix that was introduced in Section 3.1. The term $\frac{\partial f_i}{\partial \tilde{\mathbf{X}}}$ represents the derivatives with respect to the *physical* design variables, as presented in detail in Appendix A.

4. Numerical examples

In this section we demonstrate the ability of the proposed method to reduce concrete volume in slabs by optimizing the column locations. Additionally, the results presented here demonstrate the critical trade-off between the structural efficiency and the architectural cost and emphasize the importance of collaboration between architects and engineers at early stages of the project. The first example is a fairly simple design problem that validates the proposed optimization method and illustrates the sensitivity of the slab thickness to the exact column location. The other two examples are inspired by real projects with more complicated geometries and demonstrate the ability of the proposed method to contribute to concrete savings in complex, real-life projects.

Table 1. Material properties and other design parameters used in the current study

symbol	value	units	description
d_s	0.025	[m]	concrete cover
f_{cd}	17.40	$[MPa]$	concrete compression design strength
E	30000	$[MPa]$	concrete modulus of elasticity
ν	0.3	[-]	concrete Poisson's ratio
γ	$5/6$	[-]	shear strain correction factor
Δg	4	$[kN/m^2]$	dead load
q	1.5	$[kN/m^2]$	live load
γ_c	25	$[kN/m^3]$	concrete weight density

4.1. Example 1: Single Column Optimization

Considering structural design of residential apartments, it is often that most of the columns and other supporting elements are predefined at the early stages of the design according to architectural considerations. However, some freedom of the layout of the supporting elements remains also in the later stages of the design when the structural considerations are added. Thus, in this example we wish to present the optimization of a single column location in an apartment located in a typical residential tower. The floor and all dimensions are plotted in Figure 1a, where the columns have square cross section with $0.35[m]$ side lengths. In addition to the column being optimized, the boundary conditions of the floor include seven other columns along the contour of the floor, symmetry boundary conditions along the inner edges, and a portion of an internal core with wall thickness of $0.25[m]$, that is modeled with nodal pinned supports. The floor is discretized with 3800 elements and is subjected to additional external loads as listen in Table 1. The design space includes the column location, which can be anywhere within the apartment as marked by the hexagonal pattern in Figure 1a and represented by the coordinates x_c and y_c. Additionally, the thickness of the slab h is included in the design space, which may vary between minimum and maximum values $h_{min} = 0.05[m]$ and $h_{max} = 0.5[m]$, respectively.

After solving the optimization problem of Eq. (4), the optimized column location is $(x_c, y_c) \approx (10.3, 5.6)[m]$ and the corresponding slab thickness is $h = 0.228[m]$, which leads to concrete volume of $V = 49.9\left[m^3\right]$. The optimized column location as well as the resultant deflection w, and the relative deflection δ, are presented in Figures 1b and 1c, respectively. In these figures, the filled gray square is the optimized column, the hollow gray squares are the non-design columns and the gray line represents the supporting core walls.

It is apparent from the deflection maps that the optimization created three distinct spans within

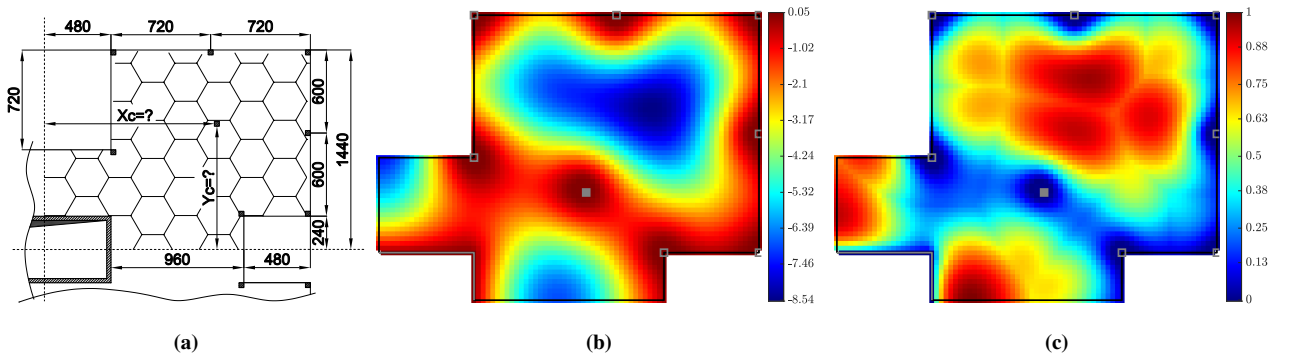

Fig. 1. Problem setup for the single column optimization problem and resultant deflections maps for the optimized column location. (a) A portion of a floor plan representing a corner apartment with a single column to be optimally located. Other columns along the outer boundaries and a section of the internal core are predefined. All dimension are in $[cm]$ (b) Deflection map $w[m]$, (c) relative deflection δ. It can be seen that the deflection constraint is active and presents a "fully deflected" behavior.

the slab. Inspecting Figure 1c, it is evident that the maximal deflection at all three spans reaches the maximal allowed deflection and thus utilizing effectively the feasible space. In a theoretical fully utilized feasible space, the deflection at every point would be equal to the allowed deflection and the relative deflection would be equal to one. Thus, the mean relative deflection may indicate the effectiveness of the design, in this case we have $\bar{\delta} = 0.516$.

As discussed in Section 3.6, after optimizing with the deflection constraint only, we check the optimized design for the design limit state requirements, namely: shear and bending resistance. Figure 2 presents the normalized W&A moments distributions and the normalized shear forces. Thus, the value one (minus one), means that the positive (negative) moment or shear at the considered point reaches the allowed value. The maximal and minimal normalized moments are $\mu_{max} = 0.3646$ and $\mu_{min} = -0.8706$, indicating that the moments are strictly within the allowable range although no constraint on the moment was imposed. This is expected in regular flat slabs and justifies the adopted optimization sequence. The normalized shear stress almost reaches the allowable shear stress value with $\tau_{ts,max} = 0.985$. In fact, in one node the shear stress exceeds the allowable value. However, this node has a rigid support representing the core, and therefore the shear stresses are overestimated and can be disregarded. Thus, although a shear constraint has not been added, the shear stresses remain within the allowable limits.

Once the optimized column location has been found, we verify it by manually investigating the design space. Thus, we generate an optimal surface by finding the minimum required slab thickness for every column location. We discretize the design space of the column location on a grid with $0.3[m]$ steps and perform the optimization at each such point by fixing the column location and allowing only the slab thickness to vary throughout the optimization. Figure 3a presents the optimal surface, where

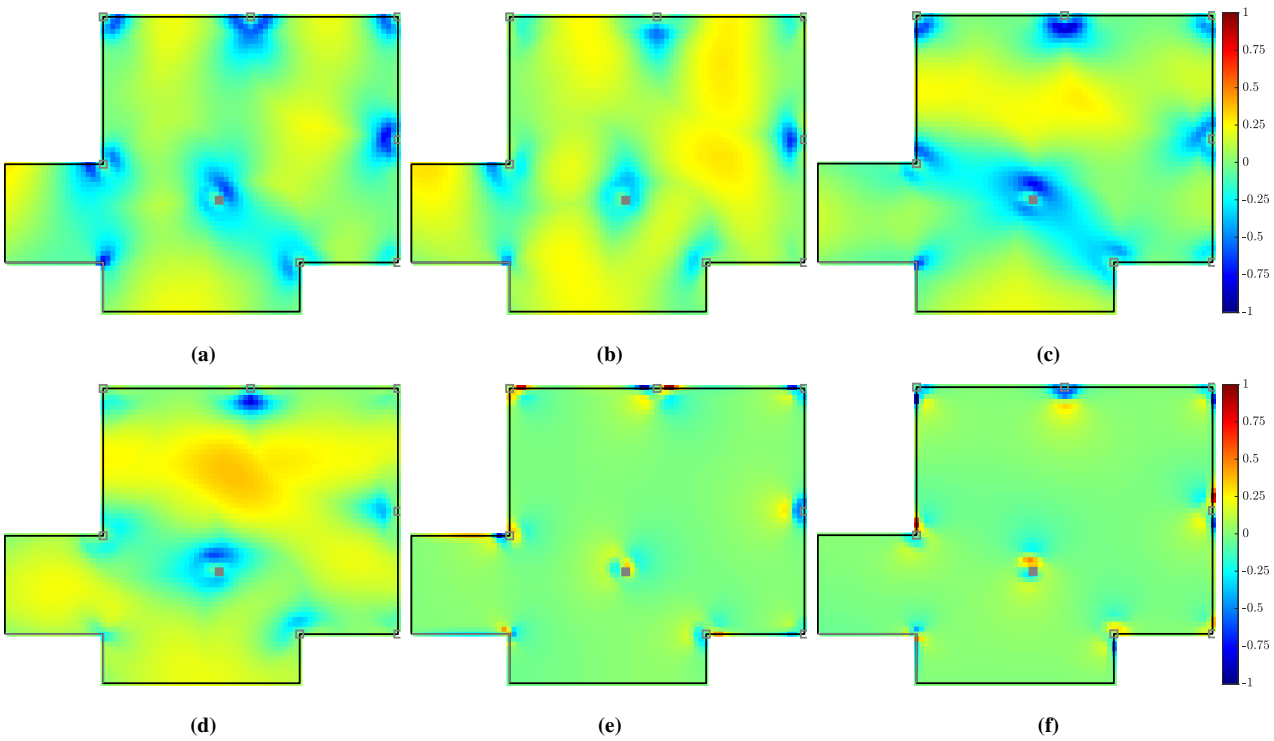

Fig. 2. Normalized moments and shear forces in design limit state. (a) $\mu_{rx,max}$, (b) $\mu_{rx,min}$, (c) $\mu_{ry,max}$, (d) $\mu_{ry,min}$, (e) τ_{xz}, (f) τ_{yz}. As expected, the bending moments are smaller than the moment capacity with $\mu_{max} = 0.3646$ and $\mu_{min} = -0.8706$ for the positive and negative moments, respectively. The shear stress nearly reaches the allowable values with maximal value of $\tau_{ts,max} = 0.985$.

the color of each pixel represents the required slab thickness for a column located at the centre of the pixel. The filled gray square is the optimized column location as obtained from the straightforward optimization and it is evident that it is located at the optimum. In fact, the minimal required thickness obtained by the optimization is slightly smaller than the minimal value obtained by the design space exploration, probably due to the continuous nature of the design variables $[x_c, y_c]$.

In order to quantify the obtained concrete savings by the optimization, a reference design is needed. Thus, we performed a poll among 26 practicing structural engineers and asked them where would they locate the column, ignoring any architectural considerations. The black crosses in Figure 3a represent the answers received from the participants of the poll, where the numbers indicate multiple answers for a certain location. It can be seen that most participants located the column approximately at the intersection of the imaginary (dotted) grid lines, trying to reduce deflections of the main span. These results show that the optimal column location is not trivial, even in a simple floor geometry. For each column location suggested by the participants of the poll, we computed the required slab thickness based on the distance to the closest data point on the optimal surface. The results vary between $h_{ref} \in [0.2688, 0.2987][m]$ with a mean value of $\bar{h}_{ref} = 0.2823[m]$. Thus, we can say that the concrete consumption saving varies between 0% in the unlikely case that the column was originally

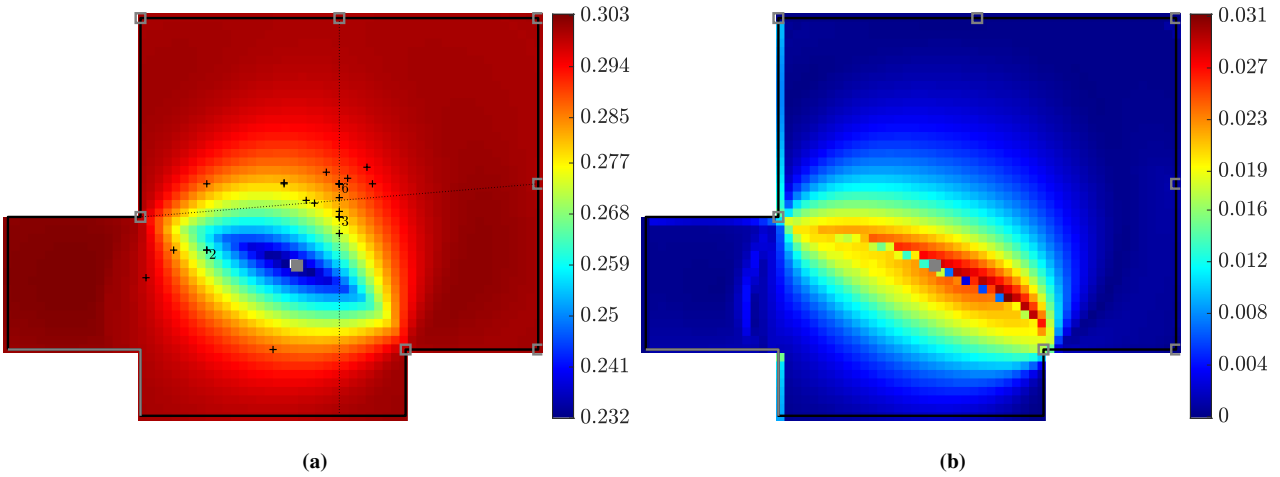

(a) **(b)**

Fig. 3. Investigation of the entire design space of (x_c, y_c), each pixel is 0.3×0.3 $[m]$. (a) Required slab thickness $h[m]$ for each column location with minimal value of $h = 0.2322$ $[m]$. The gray filled square represents the formally optimized column location, which indeed is located at the optimum and corresponds to concrete savings of 23.4%. The black crosses are the suggested locations for the column, as obtained by 26 practicing structural engineers, and show that the optimal column location is not trivial. (b) Gradient of the required thickness, representing the local potential for reduction in the thickness at each point. It can be seen that even small changes in the column location may lead to 10%-15% reduction in slab thickness.

located at the most efficient location, and 23.8% when considering $\bar{h}_{ref}$.

Figure 3b plots the design gradient, which is the local possible reduction of the thickness at each point. Considering for example a column located in the red area of the colormap in Figure 3b, the slab thickness may be reduced by three centimeters, or about 10%, when shifting the column by 1 $[m]$ in the appropriate direction. Thus, the exploration of the design space illustrates the sensitivity of the slab thickness to changes in the column location. In other words, even small changes in a single column location – that could be acceptable from an architectural standpoint – can reduce the thickness of the supported slab by 10%.

As the design freedom increases, it is expected that the optimization will find better solutions. A natural possibility to enrich the design space in our problem is to allow more columns to be optimized. Thus, we minimized the volume of the floor again, optimizing the location of two, three and eight (all) columns. Figure 4 presents the optimized column layouts and the resultant relative deflection maps. As expected, the minimal slab thickness reduces with the increase in the number of columns being optimized. Thus, optimizing two, three and eight locations of columns leads to slab thicknesses of $0.2174[m]$, $0.1836[m]$ and $0.1342[m]$, respectively. These correspond to a maximal reduction of the thickness relatively to $\bar{h}_{ref}$ of 23.0%, 35.0% and 52.5%, respectively.

We note that the increased freedom in the design space comes with an increased challenge from the architectural point of view or simply: *architectural cost*. Thus, the architectural cost refers to all

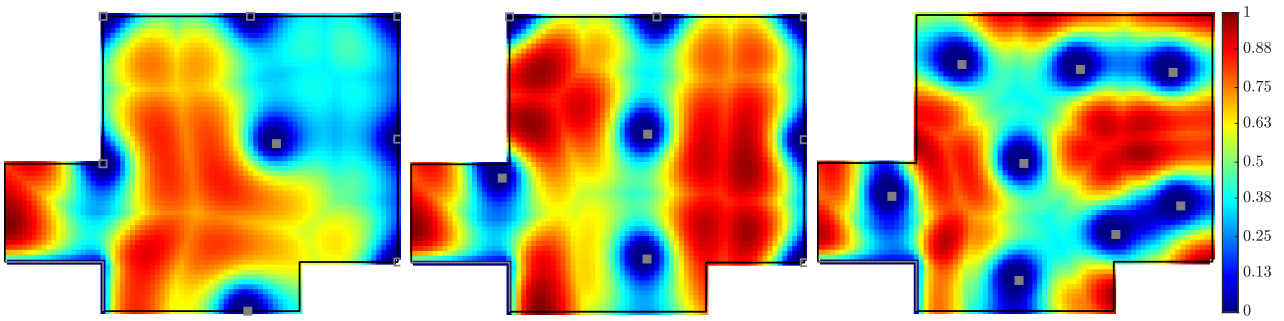

(a) **(b)** **(c)**

Fig. 4. Increased richness of the design space leads to greater savings in concrete volume. Color maps present the relative deflections, the filled gray squares represent optimized columns, other columns remain unchanged throughout the optimization and are marked with hollow gray squares. (a) Optimizing the locations of two columns, $h = 0.2174\,[m]$, $V = 47.58\,[m^3]$. (b) Optimizing the locations of three columns, $h = 0.1836\,[m]$, $V = 40.18\,[m^3]$. (c) Optimizing the locations of eight columns, $h = 0.1342\,[m]$, $V = 29.37\,[m^3]$.

necessary modifications in the architectural design due to the change in the column locations, such as updating the layout of internal walls. While the optimal single column location probably has very low architectural cost, the architectural cost with all columns being optimized is expected to be high. Thus, a general trade-off between the concrete savings, or structural efficiency, and the architectural cost is expected. An explicit quantification of the architectural cost is not straightforward and is not included in the scope of this research. Nevertheless, in the following examples the architectural cost will be considered qualitatively and implicitly.

4.2. Example 2: Irregular Residential Floor

In the previous section we showed that enriching the design space by considering more columns in the optimization, increases the potential concrete savings. In this section, we present an investigation of the relation between the design freedom and the potential concrete savings. We approach this issue by examining the effect of the maximal allowed modification to the locations of columns, compared to a reference configuration – namely, a given architectural plan. We introduce a parameter Δ_{max} that defines the maximal allowed change in a column location with respect to the reference design.

The selected floor plan in this example is inspired by a floor geometry that was presented by He et al. [38] in the context of yield line identification. This is an irregular floor in a residential building, supported by 19 square columns with side length of $0.35[m]$ and several walls, as can be seen in the general plan in Figure 5a. All geometrical data, including the column locations, is given as Supplementary Material to this paper. The thickness of the walls is $0.25[m]$ and they are modeled with nodal pinned supports that are added to all nodes within the projection area of the walls on the FE mesh. To ensure that all walls will be modeled, the distance between adjacent nodes of the FE mesh

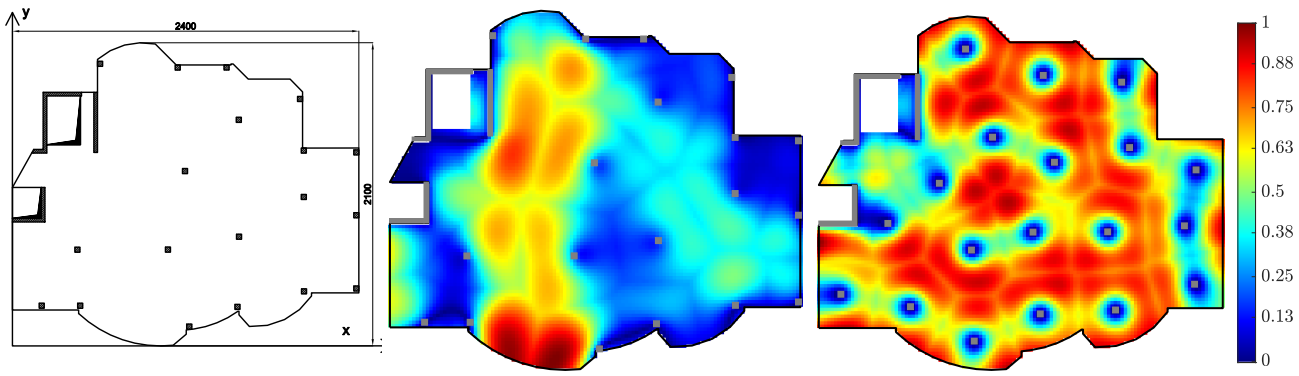

(a) (b) (c)

Fig. 5. Geometry and relative deflection δ for example 2. (a) A general plan of an irregular floor of a residential building, with the reference layout of columns, dimensions are in $[cm]$. (b) Reference column layout with optimized slab thickness of $h = 0.2226[m]$. (c) Optimized design with all constraints included. The resultant slab thickness is $h = 0.1126[m]$, which represents concrete savings of 49.4%.

should be less than the thickness of the walls. Thus, the FE mesh consists of square elements with $0.2[m]$ side length, resulting in a total of 9,224 elements. The applied forces and other parameters are the same as in the previous example. For convenience, all numerical results discussed herein are summarized at the end of this section in Table 2.

As a reference design, we adopt the column layout presented in [38], and locate the columns at the centroids of the columns therein. Thereafter, we obtain the reference slab thickness by optimizing only the slab thickness while keeping the column locations fixed. We label this reference design as $\Delta_{max} = 0$. The required thickness for the reference design is $h_{ref} = 0.2226[m]$ and the corresponding concrete volume is $V_{ref} = 82.15\ [m^3]$. Figure 5b depicts the relative deflections, whereas the rest of the results are summarised in the first row of Table 2. It can be seen that only the deflection constraint is active, therefore another optimization with all constraints was not necessary. However, the relative deflection in most regions of the slab is less than 1.0, with $\bar{\delta} = 0.376$ and one span clearly governing the design.

The optimal column layout is achieved when the columns are free to move. Thus, we include all design variables and optimize without any limitation on the design variables (except for the design domain boundaries) and label this case as $\Delta_{max} = \infty$. As before, we optimize only with the deflection constraint, which results in slab thickness of $h^*_\infty = 0.1133[m]$. However, this time the moment and shear stresses exceed the desired values and therefore re-optimization is required, and hence the * mark. After re-optimizing, all the constraints are satisfied with both the deflection and moment constraints being active. The obtained slab thickness is $h_\infty = 0.1126$, which represents substantial concrete savings of 49.4%. This thickness is slightly lower than h^*_∞, indicating that the optimization

with only the deflection constraint converged to a local minimum, which is not unlikely in non-convex optimization. Nevertheless, in most cases adding more constraints leads to higher (worse) objective function values, as will be apparent in the following.

It is evident from Figure 5c, which depicts the relative deflections of the optimized design, that the deflection in many regions of the slab approaches the allowable deflection, and consequently $\bar{\delta} = 0.638$. Moreover, it can be seen that many of the columns have concentric circles around them, indicating that the optimization tries to locate the columns such that the slope of the deformed slab will be zero above the columns. This observation is in concurrence with other studies dealing with supports optimization, for example [39, 29]. Thus, we can estimate the maximal theoretical mean relative deflection, $\bar{\delta}_{max}$, by considering representative cases of fixed-fixed and cantilever beams, which have known analytical deflection curves. Following the reasoning in Section 3.3, the allowed deflections are linear functions with zero value at the supports, where the ratio between the actual and allowed deflections are the relative deflections. Next, we integrate the relative deflections along the beams, and divide by the beam lengths for both cases, which yields $\bar{\delta} \cong 0.77$ and $\bar{\delta} \cong 0.64$, respectively. Therefore, we can assume that $\bar{\delta}_{max} \in [0.64, 0.77]$.

Another interesting observation from Figure 5c is that the columns are distributed almost uniformly with small differences between bay lengths. The reason for this is that large differences in adjacent bay lengths result in non-zero slope of the deflection surface, and therefore are generally not optimal. Thus, we expect optimized column layouts to be characterised with relatively uniform distribution, which can be used to set a good initial design. Interestingly, since the effect of pattern loading reduces with the difference between bay lengths, including pattern loading in the formulation could result in larger savings in concrete volume. Therefore, the obtained savings are possibly somewhat on the conservative side.

Next, we investigate how the design space freedom impacts the optimum, by conducting a series of optimizations with increasing values of Δ_{max}. Thus, each column is allowed to move only within a local box that is centered at the reference location of this column and has side lengths of $2\Delta_{max}$. We begin with $\Delta_{max} = 0.1[m]$, which is a very minor adjustment of the column locations and probably has very little architectural cost. The optimized slab thickness is $h = 0.2109[m]$ which reflects a reduction of 5.3% in concrete volume with respect to the reference design. Again, the deflection constraint is the only active constraint and re-optimization is not necessary.

Increasing Δ_{max} further leads to greater savings in concrete volume, as can be seen in Figure 6 that depicts the concrete volumes for different values of Δ_{max}. The color maps in Figure 6 display the relative deflections for $\Delta_{max} = \{0, 0.5, 3, \infty\}$ and it is noticeable that the efficiency, measured by $\bar{\delta}$, increases with the design freedom. Starting from $\Delta_{max} = 1.1[m]$ the moment and shear values exceed

the desired threshold when optimizing without the design limit state constraints. After re-optimizing, the designs meet all constraints and generally have slightly worse objective function value or higher concrete volume, as expected. However, for $\Delta_{max} = 3.0$ the re-optimized design is a slab with slightly smaller thickness than the thickness obtained with the deflection constraint only, which indicates again convergence to a local minimum in the latter case. In Table 2 and in Figure 6, the optimization trials that were re-optimized are marked with an asterisk.

Furthermore, We note that the optimizations with $\Delta_{max} = 4.0$ and $\Delta_{max} = 5.0$ converged to the same optimum. A possible explanation for this is the non-convexity of the optimization problem. Thus, the optimal solution might have a discrete dependence on the design space freedom. This could also explain why the optimal concrete volume that corresponds to $\Delta_{max} = \infty$ is lower than one would expect based on the graph in Figure 6.

Finally, since Δ_{max} can be regarded as a measure of the architectural cost, the curve in Figure 6 can be interpreted as the trade-off between the architectural cost and the concrete volume. Interestingly, the curve is convex and therefore small increase in the architectural cost with respect to a traditionally obtained reference design, may lead to significant reduction in concrete volume. For example, allowing $\Delta_{max} = 0.9$ results in almost 30% reduction.

4.3. Example 3: Rounded Triangular Floor

The third example that we present is inspired by another floor plan of an actual building that was presented in [40] in the context of post-tensioning optimization. This example provides another indication for the ability of the proposed method to deal with real-life problems characterized by many columns as well as non-convex shapes of floors. Additionally, we will investigate the sensitivity of the slab thickness to the exact optimized column location.

The floor has a triangular shape with rounded corners and has three rectangular openings. The boundary conditions of the floor include 19 square columns and a central concrete core with wall thickness of $0.35[m]$. Accordingly, the plate is modeled with 7,773 square elements with $0.333[m]$ side length. All other parameters are the same as in the previous example. Figure 7a depicts the floor plan and some measures, whereas all geometrical data can be found in the Supplementary Material section.

The reference layout of the columns follows the general layout in [40], as shown in Figure 7a. As before, we fix the column locations and optimize only the thickness to find the reference thickness. Thus, the optimized thickness of the slab is $h_{ref} = 0.331[m]$ and the total volume of the concrete is $V_{ref} = 285.81\left[m^3\right]$. In Figure 7b we present the relative deflections and it can be seen that the deflections at broad areas of the floor are lower than the allowable deflections, yielding $\bar{\delta}_{ref} = 0.331$.

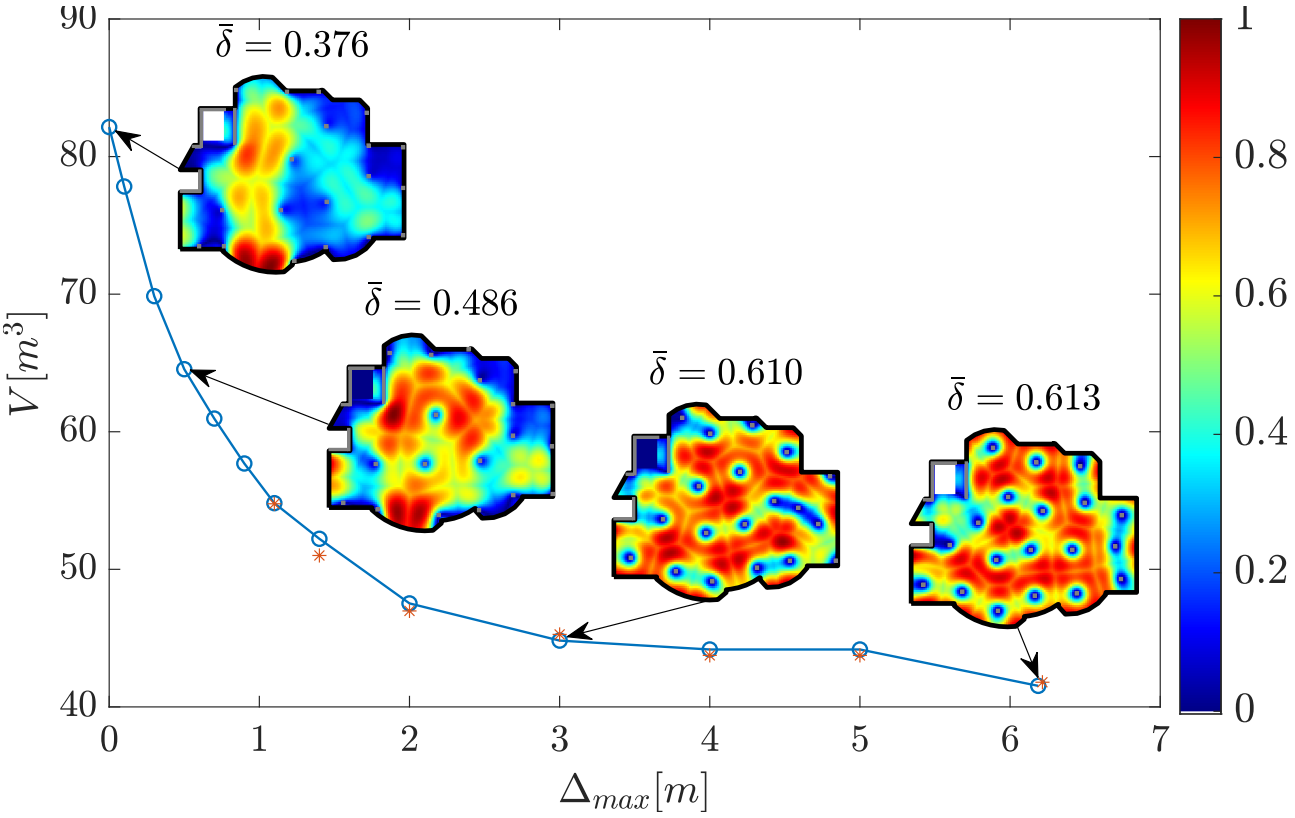

Fig. 6. Optimized concrete volume for different values of Δ_{max}. The steep slope at low values of Δ_{max} indicates that even a small update of the column layout can significantly affect the concrete volume. The red asterisks represent infeasible optimization results that were obtained with the deflection constraint only. Increasing the design freedom results in larger concrete savings that reach 49.4%. The color maps present the distribution of the relative deflection, δ, for $\Delta_{max} = \{0, 0.5, 3.0, \infty\}$. It is evident that increasing Δ_{max} results in more efficient design with higher $\bar{\delta}$.

Table 2. Optimization of the irregular slab with increasing level of design freedom. * Indicates infeasible result obtained with deflection constraint only.

$\Delta_{max}[m]$	$h[m]$	$V\left[m^3\right]$	concrete savings	$\max(\delta)$	min $\mu_{rx,min}$	max $\mu_{rx,max}$	min $\mu_{ry,min}$	max $\mu_{ry,max}$	max τ_{xz}	max τ_{yz}
0 (ref)	0.22263	82.146	-	1	-0.67985	0.3804	-0.70334	0.2245	0.52982	0.75332
0.1	0.21093	77.829	5.3%	0.99999	-0.69394	0.38755	-0.7574	0.23847	0.53367	0.72114
0.3	0.18932	69.856	15.0%	1.0004	-0.78447	0.40755	-0.85335	0.27937	0.52417	0.68032
0.5	0.17493	64.546	21.4%	1.0004	-0.83388	0.39449	-0.89157	0.33781	0.49417	0.69444
0.7	0.16521	60.958	25.8%	1.0005	-0.83793	0.38152	-0.91871	0.37442	0.47292	0.80518
0.9	0.15636	57.693	29.8%	1.0001	-0.86344	0.40016	-0.94911	0.39103	0.53638	0.94594
1.1*	0.14842	54.765	33.3%	1	-0.90331	0.41205	-1.0701	0.40226	0.6752	1.0925
1.1	0.14855	54.808	33.3%	0.99992	-0.90091	0.41236	-0.9986	0.39896	0.67933	0.99681
1.4*	0.13825	51.007	37.9%	0.99981	-1.0458	0.46773	-1.1699	0.42389	0.87382	1.1164
1.4	0.14153	52.219	36.4%	0.99791	-0.93667	0.55586	-0.99993	0.41993	0.63665	0.84977
2.0*	0.12732	46.976	42.8%	0.99931	-1.2146	0.49726	-1.1447	0.46601	1.1343	0.93098
2.0	0.12881	47.524	42.1%	0.99773	-0.95245	0.50243	-0.99964	0.46274	0.77647	0.7813
3.0*	0.12269	45.269	44.9%	0.99972	-1.0186	0.51584	-1.0952	0.54742	0.55626	0.79357
3.0	0.12148	44.82	45.4%	1.0008	-0.94927	0.59244	-0.99991	0.54407	0.55409	0.82564
4.0*	0.11856	43.745	46.8%	0.99616	-1.0396	0.59132	-1.1143	0.5098	0.58239	0.74365
4.0	0.11973	44.174	46.2%	0.99598	-0.92558	0.60812	-0.99945	0.48057	0.57248	0.6762
5.0*	0.11856	43.745	46.8%	0.99616	-1.0396	0.59132	-1.1143	0.5098	0.58239	0.74365
5.0	0.11973	44.174	46.2%	.99598	-0.92558	0.60812	-0.99945	0.48057	0.57248	0.6762
∞	0.11327	41.793	49.1%	1.0004	-1.1488	0.58745	-1.3416	0.52817	0.69394	1.0293
∞*	0.11256	41.531	49.4%	0.99992	-0.94673	0.52139	-1.0006	0.50141	0.57633	0.77411

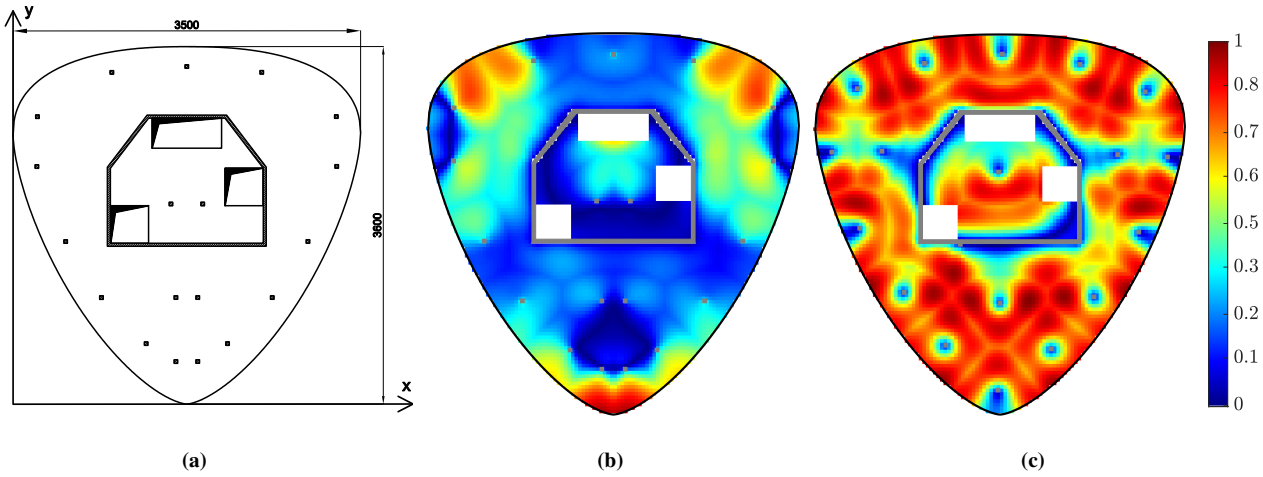

Fig. 7. Optimization of a rounded triangular floor. (a) Floor plan, with the reference layout of the columns. Dimensions are in $[cm]$. (b) Relative deflection of the reference design with $h_{ref} = 0.331[m]$. The deflections reach the allowable value only in few regions of the floor, indicating sub-optimal design. (c) Relative deflection of the optimized design with $h = 0.1836[m]$. The deflections reach the allowable value in many areas of the floor, thus indicating good utilization of the feasible space. Surprisingly, one column merged with the core walls, thus practically eliminating this column.

Re-optimization is not necessary because the design limit state requirements are met. Specifically, the relative maximal and minimal moments in x and y directions are $\mu_{rx,max} = 0.252$, $\mu_{rx,min} = -0.451$, $\mu_{ry,max} = 0.220$, $\mu_{ry,min} = -0.320$, and the maximal relative transverse shear stress is $\tau_{rs,max} = 0.53$.

After establishing the reference design, we optimize the same floor with the reference design as an initial design. The optimized slab thickness is $h = 0.1836[m]$ and the resultant concrete volume is $V = 158.607\,[m^3]$, which represents a volume saving of 44.5%. Figure 7c presents the relative deflection map and the optimized column layout, which is quite different from the reference layout in Figure 7b. Quite surprisingly, one of the columns that was originally located inside the core has merged with the core wall. Thus, the column is not active and the optimization effectively converged to a solution with fewer columns. Comparing the relative deflections of the reference and the optimized designs, the improved structural efficiency is clear with $\bar{\delta} = 0.626$. The optimized design meets the moment and shear constraints and re-optimization was not needed. However, the moments and shear stresses are closer to the desired values with $\mu_{rx,max} = 0.394$, $\mu_{rx,min} = -0.786$, $\mu_{ry,max} = 0.415$, $\mu_{ry,min} = -0.759$, $\tau_{xz} = 0.67$, and $\tau_{yz} = 0.66$. This provides another indication for better utilization of the feasible space.

Similarly to the first example, we wish to investigate the sensitivity of the slab thickness to the column locations. However, because we optimize the location of many columns concurrently, investigation of the entire design space is not practical. Therefore, in this example we investigate the sensitivity of the slab thickness using random perturbations of the optimized design with increasing amplitude. For this purpose, we add a random noise with normal distribution and maximal amplitude

of ξ to the coordinates of the optimized columns. Thereafter, we optimize the slab thickness, keeping the column locations fixed. We consider five values for the amplitude $\xi \in \{0.1, 0.2, 0.3, 0.4, 0.5\}$ and for each value we perform 50 random perturbations resulting in a total of 250 perturbations of the optimized design.

Figure 8a presents the 250 results, where the horizontal axis is the slab thickness, the vertical axis is the mean relative deflection, the colors represent different magnitudes of perturbation, and the black asterisk is the optimized design without any perturbation. The first thing that can be noticed from the results is that the optimized design outperforms all perturbed designs, providing an indication of a successful convergence of the optimization to a good local minimum. Another clear observation – which is expected – is the relation between the slab thickness and the mean relative deflection $\bar{\delta}$. Thus, reduction of the thickness of the slab is achieved by increasing the relative mean deflection. A result that is less obvious, is the potential volume saving when perturbations are performed with respect to the optimized design. Even relatively large changes in locations with $\xi = 0.5$ give a slab thickness of up to $h = 0.24[m]$, corresponding to roughly 38% less volume. In the trade-off between structural efficiency and architectural cost, the perturbation can be seen as a way to retain the architectural freedom, based on a starting point that has the best structural efficiency. This view complements the discussion of the previous example, where the trade-off was expressed as potential savings for diverging from the original architectural plan.

In Figure 8b we present the same data in a slightly different way, to illuminate the sensitivity of the slab's thickness to the column locations. The vertical axis is the required increase in slab thickness relatively to the optimized design, Δh, and hence the vertical bars represent the distribution of the increase in thicknesses for each magnitude of the perturbation, where the circles mark the average. The blue line connects the average thicknesses and depicts the sensitivity of the slab thickness to the column locations. Alternatively, if we consider ξ as a measure of the architectural freedom, this figure presents the structural cost of the architectural freedom. Thus, emphasizing the importance of early collaboration between architects and engineers.

5. Discussion and conclusions

We presented a method to minimize the concrete consumption in slabs by optimizing the column locations, and then use it to investigate the sensitivity of the thickness to the column locations. The optimization method considers the deflections as well as the moment and shear capacities. For any given floor plan, the method generates an optimized layout of columns and the corresponding minimal required slab thickness. We use gradient-based optimization with analytically derived sensitivities, which results in a very effective numerical method that can be used for problems with a large number

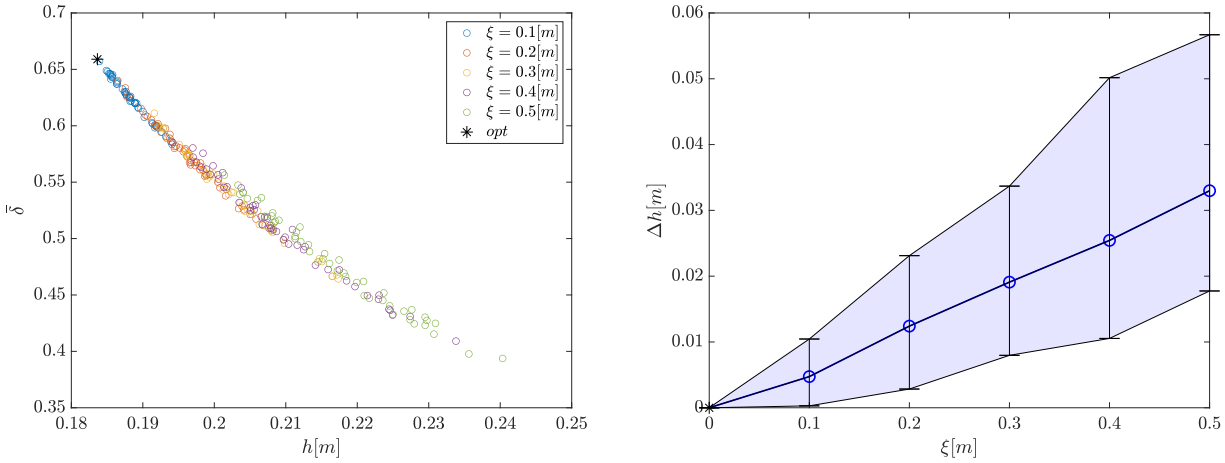

(a) **(b)**

Fig. 8. Investigating the sensitivity of the slab thickness to the exact locations of columns, in the optimization of a rounded triangular floor. All results indicate significant reduction of the thickness with respect to the reference design ($h_{ref} = 0.331[m]$), where the black asterisk represents the optimum without any perturbation and corresponds to slab thickness reduction of 44.5%. (a) A scatter of all perturbations of the optimum manifests a clear relation between the required slab thickness h and the mean relative deflection $\bar{\delta}$. (b) The spread of the increase in slab thicknesses Δh obtained for different magnitudes of the perturbation ξ, where the mean values are marked with circles and visualizing the sensitivity of the slab thickness to the exact column location. For example, a perturbation of up to $0.5[m]$ in the optimized column locations leads to increase in the required slab thickness of $3.3[cm]$ (or almost 18%) on average. Additionally, the figure illustrates the trade-off between the architectural freedom, represented by ξ, and the structural cost, represented by the required increase in slab thickness Δh.

of design variables, that would have not been practical with zero-order optimization methods. For example, simultaneous optimization of a large number of columns within an extended framework that includes also the column dimensions and a slab with varying thickness.

Through three different design examples, we showed that traditional column layouts, or layouts that are based mainly on architectural considerations, are far from optimal and that the slab thickness can be reduced by up to 50% by optimizing the column locations. Moreover, we show that even small changes in the column locations with respect to the architectural plan, in the order of $0.1[m] - 0.5[m]$, may lead to savings in the range of $5\% - 20\%$.

The results of this study indicate that the optimal column layout is not trivial and that traditional design is usually sub-optimal. As a consequence, collaborative architectural and structural design from the preliminary stages when the column layout is determined, is key to achieve significant concrete savings. Additionally, the results of this study show that the slab thickness is very sensitive to the precise column locations. Considering that small updates in column locations, especially if introduced in the early stages of the design, likely to have minimal architectural cost, concrete savings of up to 20% in slabs can be achieved for most buildings. More pronounced modifications in column locations will probably lead to greater savings of concrete, but might have some architectural cost that should be considered. This could be accomplished by defining an allowable design domain for each column, such that the architectural cost is acceptable.

Another interesting observation that can be made is the direct relation between the optimality of the column layout and the rate at which the deflection constraint is satisfied. Thus, the mean relative deflection can be used as an indicator for the effectiveness of a design, with an estimated theoretical maximum value in the range $\bar{\delta}_{max} \in [0.64, 0.77]$.

Throughout this research the architectural cost has been considered qualitatively and the natural trade-off with the structural efficiency was demonstrated. Explicit, quantitative consideration of the architectural cost is an interesting direction for future research. Additionally, although a substantial reduction in concrete volume is possible by the proposed method, it is possible that more steel reinforcement will be needed. Thus, the optimal balance between concrete and steel in terms of cost and environmental impact still remains open for future work. Furthermore, including also non-linear material response and plasticity might reveal interesting failure modes.

6. Data Availability Statement

Some or all data, models, or code that support the findings of this study are available from the corresponding author upon reasonable request.

7. Acknowledgments

This research was funded by the Ministry of Construction and Housing, Israel. The financial support is gratefully acknowledged.

Appendix A. Sensitivity analysis

Since we implement gradient based optimization, the first-order derivatives should be provided. In this section we present in detail all calculations involved in the computation of these derivatives. We note that the analytical sensitivities were verified by comparing to numerical derivatives obtained with finite differences method and were found to be accurate.

The derivatives with respect to the mathematical design variables are obtained by the chain rule

$$\frac{\partial f_\alpha}{\partial \mathbf{X}} = \frac{\partial f_\alpha}{\partial \tilde{\mathbf{X}}} \frac{\partial \tilde{\mathbf{X}}}{\partial \mathbf{X}}, \quad \text{with} \quad \alpha \in \{0, 1, 2, 3\}, \tag{A.1}$$

where $\frac{\partial \tilde{\mathbf{X}}}{\partial \mathbf{X}} = \mathbf{N}^{-1}$ is the Jacobian matrix, and $\frac{\partial f_\alpha}{\partial \tilde{\mathbf{x}}}$ are the derivatives of the α functional with respect the physical design variables and discussed in following sub-sections.

Appendix A.1. Volume Objective function

The sensitivities of the volume can be obtained explicitly because it does not depend on the structural response. Thus, we differentiate Eq. (13)

$$\frac{\partial V}{\partial \tilde{X}} = \sum_{\ell=1}^{N_\ell} \frac{\partial h_\ell}{\partial \tilde{X}} A_\ell, \tag{A.2}$$

where $\tilde{X}$ is any of the physical design variables. The derivative of the elemental thickness h_ℓ with respect the slab thickness is simply $\frac{\partial h_\ell}{\partial h} = 1.0$ and zero with respect the columns locations.

Appendix A.2. Deflection Constraint

In the perspective of the individual MMA iteration, the threshold value of the constraint is constant. Therefore the derivative of the deflection constraint equals to the derivative of the maximal relative deflection, scaled by $1/\hat{\tilde{\delta}}^*$

$$\frac{\partial f_1}{\partial \tilde{X}} = \frac{1}{\tilde{\delta}^*} \frac{\partial \tilde{\delta}}{\partial \tilde{X}}. \tag{A.3}$$

Thus, we focus on the derivative of $\tilde{\delta}$.

The deflection constraint is an implicit function of the design variables and therefore we adopt the adjoint approach. The basic idea is to augment the functional with the equilibrium residual multiplied by an adjoint vector that will be selected such that the implicit terms will vanish. Thus, the augmented functional is

$$\tilde{\delta}_a = \tilde{\delta} - \boldsymbol{\lambda}_\delta^T \left(\mathbf{K}\mathbf{u}_s - \mathbf{f}_s \right). \tag{A.4}$$

Since the equilibrium residual equals to zero, the augmented functional equals to the original functional and so are the derivatives.

Thus, we differentiate the augmented constraint with respect to the design variables. Keeping in mind that the deflection constraint also depends explicitly on the design variables through the allowed deflection, we get

$$\frac{\partial \tilde{\delta}_a}{\partial \tilde{X}} = \frac{\partial \tilde{\delta}}{\partial \mathbf{u}_s}\frac{\partial \mathbf{u}_s}{\partial \tilde{X}} + \frac{\partial \tilde{\delta}}{\partial \mathbf{w}_A}\frac{\partial \mathbf{w}_A}{\partial \tilde{X}} - \boldsymbol{\lambda}_\delta^T\left(\frac{\partial \mathbf{K}}{\partial \tilde{X}}\mathbf{u}_s + \mathbf{K}\frac{\partial \mathbf{u}_s}{\partial \tilde{X}} - \frac{\partial \mathbf{f}_s}{\partial \tilde{X}}\right). \tag{A.5}$$

Since the derivatives of the augmented and original functionals are the same, we switch back to the original functional. As mentioned, the adjoint vector is computed such that the terms $\frac{\partial \mathbf{u}}{\partial \tilde{X}}$ will cancel each other. Thus, the derivative of the deflection is

$$\frac{\partial \tilde{\delta}}{\partial \tilde{X}} = \frac{\partial \tilde{\delta}}{\partial \mathbf{w}_A}\frac{\partial \mathbf{w}_A}{\partial \tilde{X}} - \boldsymbol{\lambda}_\delta^T\left(\frac{\partial \mathbf{K}}{\partial \tilde{X}}\mathbf{u}_s - \frac{\partial \mathbf{f}_s}{\partial \tilde{X}}\right) \quad \text{with} \quad \mathbf{K}^T\boldsymbol{\lambda}_\delta = \left(\frac{\partial \tilde{\delta}}{\partial \mathbf{u}_s}\right)^T \tag{A.6}$$

The adjoint vector $\boldsymbol{\lambda}_\delta$ and $\frac{\partial \tilde{\delta}}{\partial \hat{\mathbf{u}}_s}$ are the same as presented in [35]. The derivative of the maximal approximated relative deflection with respect to the allowed deflection is obtained by substituting Eq. (14) into Eq. (15) and differentiating

$$\frac{\partial \tilde{\delta}}{\partial \mathbf{w}_A} = -\tilde{\delta}\left[\sum_j \delta_j^p\right]^{-1}\sum_j \delta_j^{p-1} w_j \left(w_A\right)_j^{-2}. \tag{A.7}$$

The derivative of the allowed deflections with respect to the design variables is obtained by replacing $r_{min,j}$ in Eq. (18) with its derivative, and multiplying by $\frac{1}{750}$ according to Eq. (17). Thus, by differentiating Eq. (19) we obtain the derivative of the distance form the j^{th} node to the closest column,

$$\frac{\partial r_{min,j}}{\partial \tilde{X}} = r_{min,j}\sum_i r_{ij}^{p-1}\frac{\partial r_{ij}}{\partial \tilde{X}}. \tag{A.8}$$

The derivative $\frac{\partial r_{ij}}{\partial \tilde{X}}$ is computed by differentiating the distance between the i^{th} column and the j^{th} node, where for all design variables other than the i^{th} column location, the derivative is equal to zero.

The next term in Eq. (A.6) is the derivative of the stiffness matrix with respect to the design variables, which were discussed in [29] and are brought here for completeness.

As mentioned, the stiffness matrix of the supported plate is simply summation of the plate's stiffness matrix and the equivalent matrices of the columns

$$\mathbf{K} = \mathbf{K}_p + \sum_{i=1}^{N_{col}} \mathbf{K}_{cp,i}. \tag{A.9}$$

Thus, the derivatives with respect the column locations affect only the added equivalent column stiffness matrices. Thus, by differentiating Eq. A.9 with respect the x coordinate of the i^{th} column we get

$$\frac{\partial \mathbf{K}}{\partial x_{c,i}} = \frac{\partial \mathbf{K}_{cp,i}}{\partial x_{c,i}}. \tag{A.10}$$

The derivative of equivalent stiffness matrix of the i^{th} column with respect $x_{c,i}$ is obtained by differentiating Eq. (1)

$$\frac{\partial \mathbf{K}_{cp,i}}{\partial x_{c,i}} = \sum_{j}^{N_n} \left[\frac{\partial \mathbf{K}_{cp,i}}{\partial x_{c,i}} \right]_j = \sum_{j}^{N_n} \frac{\partial w_{ij}}{\partial x_{c,i}} \mathbf{K}_{c,i}. \tag{A.11}$$

The summation sign stands for assembly according the nodal DOF. The derivative of the projection weight is obtained by differentiating Eq. (2) and substituting into Eq. (3),

$$\frac{\partial w_{ij}}{\partial x_{c,i}} = \frac{\frac{\partial \tilde{w}_{ij}}{\partial x_{c,i}} \sum_k \tilde{w}_{ik} - \tilde{w}_{ij} \sum_k \frac{\partial \tilde{w}_{ik}}{\partial x_{c,i}}}{\left(\sum_k \tilde{w}_{ik}\right)^2} \tag{A.12}$$

with

$$\frac{\partial \tilde{w}_{ij}}{\partial x_{c,i}} = -\frac{\beta}{\eta} \left(\frac{r_{ij}}{\eta} \right)^{2\beta-1} \frac{\partial r_{ij}}{\partial x_{c,i}} \tilde{w}_{ij}. \tag{A.13}$$

The derivatives with respect to $y_{c,i}$ are computed in the same way.

The derivative of the stiffness matrix with respect the thickness design variable affect the plate's stiffness matrix, $\mathbf{K}_p$, and are obtained by differentiating the elemental stiffness matrices and thereafter assembling in a regular manner. The plate's stiffness matrix is assembled in a standard manner, for a mesh with identical elements

$$\mathbf{K}_p = \sum_{\ell} \mathbf{K}_\ell = \sum_{\ell} \mathbf{B}_\ell^T \mathbf{D}_\ell \mathbf{B}_\ell = \sum_{\ell} \mathbf{B}^T \mathbf{D} \mathbf{B}, \tag{A.14}$$

where $\mathbf{B}$ and $\mathbf{D}$ are the elemental generalized differentiation and constitutive matrices. Thus, after differentiating we get

$$\frac{\partial \mathbf{K}_p}{\partial h} = \sum_{\ell} \mathbf{B}^T \frac{\partial \mathbf{D}}{\partial h} \mathbf{B}, \tag{A.15}$$

where the derivative of the constitutive matrix is computed by explicit differentiation.

The final term in Eq. (A.6) is the derivative of the external forces vector with respect to the design variables. The external forces depend on the design through the thickness and the concrete mass density

$$\frac{\partial \mathbf{f}_s}{\partial h} = \sum_{\ell} \frac{\gamma_c A_\ell}{4}, \tag{A.16}$$

where γ_c is the mass density of the concrete, A_ℓ is the area of the elements, and the summation sign stands for assembly according the elemental DOF.

Appendix A.3. Shear Constraint

Similarly to the deflection constraint, the derivative of the shear constraint is,

$$\frac{\partial f_2}{\partial \tilde{X}} = \frac{1}{\tilde{\sigma}_{ts}^*} \frac{\partial \tilde{\sigma}_{ts}}{\partial \tilde{X}}. \tag{A.17}$$

Since $\tilde{\sigma}_{ts}$ is an implicit function of the design variables, we use the adjoint approach again. The augmented functional is

$$(\tilde{\sigma}_{ts})_a = \tilde{\sigma}_{ts} - \boldsymbol{\lambda}_\tau^T \left(\mathbf{K}\mathbf{u}_d - \mathbf{f}_d\right). \tag{A.18}$$

This time, there is no explicit dependence and therefore after differentiating and replacing the augmented functional with the original one, we get

$$\frac{\partial \tilde{\sigma}_{ts}}{\partial \tilde{X}} = \frac{\partial \tilde{\sigma}_{ts}}{\partial \mathbf{u}_d}\frac{\partial \mathbf{u}_d}{\partial \tilde{X}} - \boldsymbol{\lambda}_\tau^T \left(\frac{\partial \mathbf{K}}{\partial \tilde{X}}\mathbf{u}_d + \mathbf{K}\frac{\partial \mathbf{u}_d}{\partial \tilde{X}} - \frac{\partial \mathbf{f}_d}{\partial \tilde{X}}\right). \tag{A.19}$$

Selecting the adjoint vector such that the terms involving $\frac{\partial \mathbf{u}_d}{\partial \tilde{X}}$ will vanish, we get

$$\frac{\partial \tilde{\sigma}_{ts}}{\partial \tilde{X}} = -\boldsymbol{\lambda}_\tau^T \left(\frac{\partial \mathbf{K}}{\partial \tilde{X}}\mathbf{u}_d - \frac{\partial \mathbf{f}_d}{\partial \tilde{X}}\right) \quad \text{with} \quad \mathbf{K}^T\boldsymbol{\lambda}_\tau = \left(\frac{\partial \tilde{\sigma}_{ts}}{\partial \mathbf{u}_d}\right)^T. \tag{A.20}$$

The only term that is unknown is $\frac{\partial \tilde{\sigma}_{ts}}{\partial \hat{\mathbf{u}}_d}$ which is obtained by differentiation of Eq. (21)

$$\frac{\partial \tilde{\sigma}_{ts}}{\partial \mathbf{u}_d} = \hat{\tilde{\sigma}}_{ts}\left(\sum_{j=1}^{2N_{nodes}} \sigma_{ts,j}^{p}\right)^{-1} \left(\boldsymbol{\sigma}_{ts}^{\circ(p-1)}\right)^T \frac{\partial \boldsymbol{\sigma}_{ts}}{\partial \mathbf{u}_d}, \tag{A.21}$$

where $\frac{\partial \boldsymbol{\sigma}_{ts}}{\partial \mathbf{u}_d}$ is obtained by differentiating (5), multiplying with $\mathbf{W}$, and selecting the appropriate terms

$$\frac{\partial \mathbf{S}}{\partial \mathbf{u}_d} = \mathbf{W}^T\mathbf{D}\mathbf{B} \tag{A.22}$$

Appendix A.4. Moment Constraint

The derivative of the moment constraint is

$$\frac{\partial f_3}{\partial \tilde{X}} = \frac{1}{\tilde{\mu}^*}\frac{\partial \tilde{\mu}}{\partial \tilde{X}} \tag{A.23}$$

The augmented moment functional is

$$(\tilde{\mu})_a = \tilde{\mu} - \boldsymbol{\lambda}_\mu^T \left(\mathbf{K}\mathbf{u}_d - \mathbf{f}_d\right). \tag{A.24}$$

The relative moment is related to the design variables both implicitly and explicitly, $\tilde{\mu} = \tilde{\mu}\left(\tilde{X}, \mathbf{u}_d\left(\tilde{X}\right)\right)$. Therefore, we distinguish between the total derivative and the partial derivative of the relative moment by using different operators notations of d and ∂, respectively. Thus, after differentiating the above equation and getting back to the original moment functional we get

$$\frac{d\tilde{\mu}}{d\tilde{X}} = \frac{\partial \tilde{\mu}}{\partial \mathbf{u}_d}\frac{\partial \mathbf{u}_d}{\partial \tilde{X}} + \frac{\partial \tilde{\mu}}{\partial \tilde{X}} - \boldsymbol{\lambda}_\mu^T \left(\frac{\partial \mathbf{K}}{\partial \tilde{X}}\mathbf{u}_d + \mathbf{K}\frac{\partial \mathbf{u}_d}{\partial \tilde{X}} - \frac{\partial \mathbf{f}_d}{\partial \tilde{X}}\right). \tag{A.25}$$

After eliminating the derivatives $\frac{\partial \mathbf{u}}{\partial \tilde{X}}$ by finding a proper adjoint vector, the derivative of the moment constraint is

$$\frac{d\tilde{\mu}}{d\tilde{X}} = \frac{\partial \tilde{\mu}}{\partial \tilde{X}} - \boldsymbol{\lambda}_\mu^T \left(\frac{\partial \mathbf{K}}{\partial \tilde{X}}\mathbf{u}_d - \frac{\partial \mathbf{f}_d}{\partial \tilde{X}}\right) \quad \text{with} \quad \mathbf{K}^T\boldsymbol{\lambda}_\mu = \left(\frac{\partial \tilde{\mu}}{\partial \mathbf{u}_d}\right)^T. \tag{A.26}$$

The explicit derivative can be written in the following form

$$\frac{\partial \tilde{\mu}}{\partial \tilde{X}} = \frac{\partial \tilde{\mu}}{\partial h}\frac{\partial h}{\partial \tilde{X}}, \quad \text{with} \quad \frac{\partial \tilde{\mu}}{\partial h} = \tilde{\mu}\left(\sum \boldsymbol{\mu}^p\right)^{-1}\left(\frac{\partial \boldsymbol{\mu}}{\partial h}\right)^T \boldsymbol{\mu}^{\circ(p-1)}, \tag{A.27}$$

where $\circ$ indicates elementwise operation. The derivative of the relative W&A moments with respect the slab thickness is given by

$$\frac{\partial \boldsymbol{\mu}}{\partial h} = \left\{\left[\left(\frac{\partial \mathbf{M}}{\partial h}\right)^T \mathbf{M}_c - \mathbf{M}^T \frac{\partial \mathbf{M}_c}{\partial h}\right] \circ \mathbf{M}_c^{\circ -2}\right\}. \tag{A.28}$$

In the equation above, $\mathbf{M}$ is a vector with all W&A moments at all nodes and $\mathbf{M}_c$ is a vector with the moment capacities. All W&A moments have similar structure, thus for example the derivative of $M_{rx,max}$ is given by

$$\frac{\partial M_{rx,max}}{\partial h} = \frac{\partial M_{xx}}{\partial h} + \text{sign}\left(M_{xy}\right)\frac{\partial M_{xy}}{\partial h}. \tag{A.29}$$

The derivatives of the plate moments are obtained by differentiating Eq. (5), multiplying with $\mathbf{W}$, and selecting the moments components

$$\frac{\partial \mathbf{S}}{\partial h} = \mathbf{W}^T \frac{\partial \mathbf{D}}{\partial h}\mathbf{B}\hat{\mathbf{u}}_d. \tag{A.30}$$

The derivative of the moment capacities is obtained by differentiating Eq. (24), where the only derivative with non zero value is the derivative with respect the slab thickness

$$\frac{\partial \mathbf{M}_c}{\partial h} = \mathbf{1}\left(h - d_s\right)0.64 f_{cd}. \tag{A.31}$$

The last component is the derivative of the approximate maximum relative moment with respect to the displacements which is obtained by differentiating Eq. (26)

$$\frac{\partial \tilde{\mu}}{\partial \mathbf{u}_d} = \tilde{\mu}\left(\sum \boldsymbol{\mu}^p\right)^{-1}\left(\frac{\partial \mathbf{M}}{\partial \mathbf{u}_d}\right)^T \left\langle \mathbf{M}_c^{\circ -1}\right\rangle \boldsymbol{\mu}^{\circ(p-1)} \tag{A.32}$$

where $< \cdot >$ is a diagonal operator and the derivatives of the nodal moments were computed in Eq. (A.22). All other components are given in previous derivations of the SA of the other functionals.

Appendix B. Implementation

We solve the optimization problem using a gradient based algorithm due to its efficiency in dealing with large number of design variables. Specifically, the MMA algorithm [37] which is common algorithm in structural optimization. However, a successful optimization requires also several implementational techniques which are described in the following sub-sections together with some related considerations. Thereafter, we summarise all the geometrical data that is used in the examples that are presented in this study.

Appendix B.1. Convergence Criteria

The basic convergence criterion is related to the change in the objective function. Because the objective function might have noisy behavior, we consider the average change in the objective function over the previous N_{f0} iteration. We define a cumulative convergence parameter f_{0c} that is promoted each iteration that the change in average objective function is less than f_{0c}^{*} and demoted otherwise. The objective function is converged when the cumulative convergence parameter is equal to f_{0ci}. Additionally, we require that at convergence the solution is feasible, such that the maximum of all constraints is less than $f^{*} = 0.01$

Appendix B.2. Dynamic Move Limits

It was observed that the optimization may have oscillatory behavior of the design variables, and as a result the objective function, do not converge. Therefore we implement a dynamic move limit mechanism such that the move limit of an oscillating design variable is tightened and the move limit of monotonically behaving design variables gets wider. Thus, each design variable has a stability index SI that is promoted each time that the change in design variable value is the same as in the previous iteration and demoted otherwise. The stability index of the m^{th} design variable at the the n^{th} iteration is given by

$$SI_m^n = SI_m^{n-1} + \text{sign}\left[\left(X_m^n - X_m^{n-1}\right)\left(X_m^{n-1} - X_m^{n-2}\right)\right]. \tag{B.1}$$

Once the stability index of a design variable reaches the positive or negative threshold values, SI^{+} and SI^{-}, the move limit is updated accordingly as follows

$$ML_m^n = \begin{cases} ML_m^{n-1}\alpha & SI_m^n = SI^{+} \\ ML_m^{n-1}\alpha^{\left(-\frac{SI^{+}}{SI^{-}}\right)} & SI_m^n = SI^{-}\,, \quad \text{with} \quad \alpha > 1. \\ ML_m^{n-1} & \text{otherwise} \end{cases} \tag{B.2}$$

Additionally, it was observed that the oscillations may occur on a larger scale, where the design variables behave monotonically with respect the neighboring iterations but the optimization fail to converge. In order to deal with this problem we monitor the number of times that the objection function crosses the average objective function at a predefined sampling widow of iterations. Thus, we define a threshold value for the number of intersections between the average and non-average objective functions, beyond which all move limits of all design variables are narrowed down. Herein we consider two sampling windows, representing two different scales of iterations, of 10 and 100 iterations and set the threshold value of intersections to 3 and 10 respectively. Thus, each time that any of the threshold values is reached, all move limits narrowed down by factor of 0.9. Finally, we set minimum and maximum values for the move limits of 1×10^{-2} and 1×10^{-4}, respectively.

Appendix B.3. Numerical Damping And Continuation Of The Projection Radius

It was shown in [29] that the numerical performance of optimization of supports location can be significantly improved by implementing three techniques presenter therein. Namely: Control of initial design, continuation of the projection radii and numerical damping of the derivatives. In this study we implemented the numerical damping and the three stage continuation scheme of the projection radii as presented in [29]. The initial design control has not been implemented directly, since the initial designs herein are obtained manually and comply with the conditions of the initial control as defined in [29].

References

[1] R. M. Andrew, Global co 2 emissions from cement production, Earth System Science Data 10 (2018) pp.195–217. doi:https://doi.org/10.5194/essd-10-195-2018.

[2] C. Thirion, Putting the material in the right place: Investigations into the sustainable use of structural materials to reduce the initial embodied environmental impact of building structures, Ph.D. thesis, UCL (University College London), 2013. URL: https://discovery.ucl.ac.uk/id/eprint/1396779.

[3] W. Shanks, C. Dunant, M. P. Drewniok, R. Lupton, A. Serrenho, J. M. Allwood, How much cement can we do without? lessons from cement material flows in the uk, Resources, Conservation and Recycling 141 (2019) pp.441–454. doi:https://doi.org/10.1016/j.resconrec.2018.11.002.

[4] S. Weidner, A. Mrzigod, R. Bechmann, W. Sobek, Graue emissionen im bauwesen–bestandsaufnahme und optimierungsstrategien, Beton-und Stahlbetonbau 116 (2021) 969–977. doi:https://doi.org/10.1002/best.202100065.

[5] O. Sigmund, K. Maute, Topology optimization approaches, Structural and Multidisciplinary Optimization 48 (2013) 1031–1055. doi:10.1007/s00158-013-0978-6.

[6] J.-H. Zhu, W.-H. Zhang, L. Xia, Topology optimization in aircraft and aerospace structures design, Archives of Computational Methods in Engineering 23 (2016) 595–622. doi:10.1007/s11831-015-9151-2.

[7] T. Dbouk, A review about the engineering design of optimal heat transfer systems using topology optimization, Applied Thermal Engineering 112 (2017) 841–854. doi:https://doi.org/10.1016/j.applthermaleng.2016.10.134.

[8] D. Yeo, R. D. Gabbai, Sustainable design of reinforced concrete structures through embodied energy optimization, Energy and buildings 43 (2011) 2028–2033. doi:https://doi.org/10.1016/j.enbuild.2011.04.014.

[9] D. Yeo, F. A. Potra, Sustainable design of reinforced concrete structures through co 2 emission optimization, Journal of structural engineering 141 (2015) B4014002. doi:https://doi.org/10.1061/(ASCE)ST.1943-541X.0000888.

[10] H. Varaee, B. Ahmadi-Nedushan, Minimum cost design of concrete slabs using particle swarm optimization with time varying acceleration coefficients, World Appl Sci J 13 (2011) 2484–94.

[11] M. Aldwaik, H. Adeli, Cost optimization of reinforced concrete flat slabs of arbitrary configuration in irregular highrise building structures, Structural and Multidisciplinary Optimization 54 (2016) 151–164. doi:10.1007/s00158-016-1483-5.

[12] S. O. A. Olawale, O. P. Akintunde, M. O. Afolabi, M. A. Tijani, Design optimization of reinforced concrete waffle slab using genetic algorithm, Journal of Soft Computing in Civil Engineering 4 (2020) 46–62. doi:10.22115/SCCE.2020.224460.1195.

[13] M. A. Ismail, C. T. Mueller, Minimizing embodied energy of reinforced concrete floor systems in developing countries through shape optimization, Engineering Structures 246 (2021) 112955. doi:https://doi.org/10.1016/j.engstruct.2021.112955.

[14] M. Rady, S. Y. Mahfouz, S. E.-D. F. Taher, Optimal design of reinforced concrete materials in construction, Materials 15 (2022) 2625. doi:https://doi.org/10.3390/ma15072625.

[15] S. Eleftheriadis, P. Duffour, D. Mumovic, Bim-embedded life cycle carbon assessment of rc buildings using optimised structural design alternatives, Energy and Buildings 173 (2018) 587–600. doi:https://doi.org/10.1016/j.enbuild.2018.05.042.

[16] P. Foraboschi, M. Mercanzin, D. Trabucco, Sustainable structural design of tall buildings based on embodied energy, Energy and Buildings 68 (2014) pp.254–269. doi:https://doi.org/10.1016/j.enbuild.2013.09.003.

[17] M. Sahab, A. Ashour, V. Toropov, Cost optimisation of reinforced concrete flat slab buildings, Engineering structures 27 (2005) 313–322. doi:https://doi.org/10.1016/j.engstruct.2004.10.002.

[18] A. Nimtawat, P. Nanakorn, A genetic algorithm for beam–slab layout design of rectilinear floors, Engineering Structures 32 (2010) pp.3488–3500. doi:https://doi.org/10.1016/j.engstruct.2010.07.018.

[19] D. Shaw, J. Miles, A. Gray, Determining the structural layout of orthogonal framed buildings, Computers & Structures 86 (2008) pp.1856–1864. doi:https://doi.org/10.1016/j.compstruc.2008.04.009.

[20] P. Sharafi, L. H. Teh, M. N. Hadi, Conceptual design optimization of rectilinear building frames: A knapsack problem approach, Engineering Optimization 47 (2015) pp.1303–1323. doi:https://doi.org/10.1080/0305215X.2014.963068.

[21] A. Chepurnenko, E. Efimenko, D. Mailyan, B. Yazyev, The location of supports under the monolithic reinforced concrete slabs optimization, Magazine of Civil Engineering (2021) 10404. doi:10.34910/MCE.104.4.

[22] O. Sigmund, On the usefulness of non-gradient approaches in topology optimization, Structural and Multidisciplinary Optimization 43 (2011) 589–596. doi:10.1007/s00158-011-0638-7.

[23] J. H. Son, B. M. Kwak, Optimization of boundary conditions for maximum fundamental frequency of vibrating structures, American Institute of Aeronautics and Astronautics Journal 31 (1993) pp.2351–2357. doi:https://arc.aiaa.org/doi/pdf/10.2514/3.11935.

[24] R. Menassa, W. DeVries, Optimization methods applied to selecting support positions in fixture design, ASME Journal for Engineering for Industry 113 (1991) pp.412–418. doi:https://doi.org/10.1115/1.2899715.

[25] T. Buhl, Simultaneous topology optimization of structure and supports, Structural and Multidisciplinary Optimization 23 (2002) pp.336–346. doi:https://doi.org/10.1007/s00158-002-0194-2.

[26] Z. Jihong, Z. Weihong, Maximization of structural natural frequency with optimal support layout, Structural and Multidisciplinary Optimization 31 (2006) 462–469. doi:10.1007/s00158-005-0593-2.

[27] H. Denli, J. Sun, Optimization of boundary supports for sound radiation reduction of vibrating structures, Journal of vibration and acoustics 130 (2008). doi:https://doi.org/10.1115/1.2776345.

[28] X. Meng, T.-U. Lee, Y. Xiong, X. Huang, Y. M. Xie, Optimizing support locations in the roof–column structural system, Applied Sciences 11 (2021). URL: https://www.mdpi.com/2076-3417/11/6/2775. doi:10.3390/app11062775.

[29] Y. Zelickman, O. Amir, Optimization of plate supports using a feature mapping approach with techniques to avoid local minima, Structural and Multidisciplinary Optimization 65 (2022) pp.1–16. doi:https://doi.org/10.1007/s00158-021-03135-3.

[30] E. Reissner, The effect of transverse shear deformation on the bending of elastic plates, Journal of Applied Mechanics (1945) pp.A69–A77. doi:https://doi.org/10.1115/1.4009435.

[31] R. D. Mindlin, Influence of rotatory inertia and shear on flexural motions of isotropic, elastic plates, Journal of Applied Mechanics 18 (1951) pp.31–38. doi:https://doi.org/10.1115/1.4010217.

[32] K.-J. Bathe, Finite element procedures. ISBN: 987-0-9790049-0-2, Klaus-Jurgen Bathe, 2006.

[33] O. C. Zienkiewicz, J. Z. Zhu, The superconvergent patch recovery and a posteriori error estimates. part 1: The recovery technique, International Journal for Numerical Methods in Engineering 33 (1992) pp.1331–1364. doi:https://doi.org/10.1002/nme.1620330702.

[34] C. Européen, Eurocode 2: Design of concrete structures—Part 1-1: General rules and rules for buildings, 2004.

[35] Y. Zelickman, O. Amir, Optimization of post-tensioned concrete slabs for minimum cost, Engineering Structures 259 (2022) 114132. doi:https://doi.org/10.1016/j.engstruct.2022.114132.

[36] R. H. Wood, G. S. T. Armer, , A. Hillerborg, Teh theory of the strip method for design of slabs. (includes appendix), Proceedings of the Institution of Civil Engineers 41 (1968) pp.285–311. doi:https://doi.org/10.1680/iicep.1968.7755.

[37] K. Svanberg, The method of moving asymptotes—a new method for structural optimization, International journal for numerical methods in engineering 24 (1987) pp.359–373. doi:https://doi.org/10.1002/nme.1620240207.

[38] L. He, M. Gilbert, M. Shepherd, Automatic yield-line analysis of practical slab configurations via discontinuity layout optimization, Journal of Structural Engineering 143 (2017) 04017036. doi:https://doi.org/10.1061/(ASCE)ST.1943-541X.0001700.

[39] M. B. Fuchs, M. A. Brull, A new strain energy theorem and its use in the optimum design of continuous beams, Computers & Structures 10 (1979) pp.647–657. doi:https://doi.org/10.1016/0045-7949(79)90008-7.

[40] M. Sarkisian, E. Long, A. Beghini, R. Garai, D. Shook, R. Henoch, A. Diaz, Optimal tendon layouts for concrete slabs in buildings derived through density-based topology optimization algorithms, in: World Congress of Structural and Multidisciplinary Optimisation, Springer, 2017, pp. 1042–1053. doi:https://doi.org/10.1007/978-3-319-67988-4_79.